

Multi-soliton solutions of coupled Lakshmanan–Porsezian–Daniel equations with variable coefficients under nonzero boundary conditions

Hui-Chao Zhao(赵会超), Lei-Nuo Ma(马雷诺), and Xi-Yang Xie(解西阳)

Citation: Chin. Phys. B, 2024, 33 (**8**): 080201. DOI: 10.1088/1674-1056/ad4d64
Journal homepage: http://cpb.iphy.ac.cn; http://iopscience.iop.org/cpb

What follows is a list of articles you may be interested in

An integrable generalization of the Fokas-Lenells equation: Darboux transformation, reduction and explicit soliton solutions

Jiao Wei(魏姣), Xianguo Geng(耿献国), and Xin Wang(王鑫)
Chin. Phys. B, 2024, 33 (**7**): 070202. DOI: 10.1088/1674-1056/ad4633

Multi-soliton solutions, breather-like and bound-state solitons for complex modified Korteweg-de Vries equation in optical fibers

Zhong-Zhou Lan(兰中周)
Chin. Phys. B, 2024, 33 (**6**): 060201. DOI: 10.1088/1674-1056/ad39d7

Higher-dimensional Chen—Lee—Liu equation and asymmetric peakon soliton

Qiao-Hong Han(韩巧红) and Man Jia(贾曼)
Chin. Phys. B, 2024, 33 (**4**): 040202. DOI: 10.1088/1674-1056/ad1822

MetaPINNs: Predicting soliton and rogue wave of nonlinear PDEs via the improved physics-informed neural networks based on meta-learned optimization

Yanan Guo(郭亚楠), Xiaoqun Cao(曹小群), Junqiang Song(宋君强), and Hongze Leng(冷洪泽)
Chin. Phys. B, 2024, 33 (**2**): 020203. DOI: 10.1088/1674-1056/ad0bf4

Soliton propagation for a coupled Schrödinger equation describing Rossby waves

Li-Yang Xu(徐丽阳), Xiao-Jun Yin(尹晓军), Na Cao(曹娜) and Shu-Ting Bai(白淑婷)
Chin. Phys. B, 2023, 32 (**7**): 070202. DOI: 10.1088/1674-1056/acb9e5

Multi-soliton solutions of coupled Lakshmanan–Porsezian–Daniel equations with variable coefficients under nonzero boundary conditions

Hui-Chao Zhao(赵会超), Lei-Nuo Ma(马雷诺), and Xi-Yang Xie(解西阳)†

Department of Mathematics and Physics, and Hebei Key Laboratory of Physics and Energy Technology, North China Electric Power University, Baoding 071003, *China*

(Received 16 April 2024; revised manuscript received 15 May 2024; accepted manuscript online 20 May 2024)

This paper aims to investigate the multi-soliton solutions of the coupled Lakshmanan–Porsezian–Daniel equations with variable coefficients under nonzero boundary conditions. These equations are utilized to model the phenomenon of nonlinear waves propagating simultaneously in non-uniform optical fibers. By analyzing the Lax pair and the Riemann–Hilbert problem, we aim to provide a comprehensive understanding of the dynamics and interactions of solitons of this system. Furthermore, we study the impacts of group velocity dispersion or the fourth-order dispersion on soliton behaviors. Through appropriate parameter selections, we observe various nonlinear phenomena, including the disappearance of solitons after interaction and their transformation into breather-like solitons, as well as the propagation of breathers with variable periodicity and interactions between solitons with variable periodicities.

Keywords: soliton, Riemann–Hilbert problem, non-zero boundary conditions, coupled Lakshmanan–Porsezian–Daniel equation

PACS: 02.30.Rz, 02.30.Ik, 05.45.Yv **DOI:** 10.1088/1674-1056/ad4d64

1. Introduction

The Lakshmanan–Porsezian–Daniel equation (LPDE), as a scalar nonlinear Schrödinger(NLS)-type one, is a fundamental format for describing optical soliton propagation within single-mode optical fibers.[1,2] Besides, the equation is found to applied in diverse fields, including oceans and nonlinear optics.[3–5] Despite its significance, the solutions for the integrable LPDE remains a pivotal challenge in the soliton theory, then researchers extend the NLS-type equation to the coupled one to capture the simultaneous propagation of waves in fibers.[6–8]

When dealing with non-uniform optical fibers, employing variable-coefficient NLS-type models offers a more accurate characterization of the system compared to their constant-coefficient counterparts.[9–12] With these insights, we study a coupled variable-coefficient LPDE to delineate the concurrent propagation of nonlinear waves in non-uniform optical media,[13–18]

$$\begin{aligned}
&\mathrm{i}q_{j,t}+\sigma(t)q_{j,xx}+\zeta(t)\sum_{k=1}^{2}\left(|q_k|^2\right)q_j+\gamma_1(t)q_{j,xxxx}\\
&+\gamma_2(t)\sum_{k=1}^{2}\left(|q_{k,x}|^2\right)q_j+\gamma_3(t)\sum_{k=1}^{2}\left(q_kq_{k,x}^*\right)q_{j,x}\\
&+\gamma_4(t)\sum_{k=1}^{2}\left(q_{k,x}q_k^*\right)q_{j,x}+\gamma_5(t)\sum_{k=1}^{2}\left(|q_k|^2\right)q_{j,xx}\\
&+\gamma_6(t)\sum_{k=1}^{2}\left(q_{k,xx}q_k^*\right)q_j+\gamma_7(t)\sum_{k=1}^{2}\left(q_{k,xx}^*q_k\right)q_j\\
&+\gamma_8(t)\left[\sum_{k=1}^{2}\left(|q_k|^2\right)\right]^2q_j=0,\quad (j=1,2),
\end{aligned}\tag{1}$$

where $\sigma(t)$ represents the group velocity dispersion (GVD), $\zeta(x)$ denotes the self-phase modulation (SPM), and $\gamma_1(t)$ represents the fourth-order dispersion, while $\gamma_j(t)$ covers all coefficients related to nonlinear effects.

Extensive researches have been investigated on Eq. (1) under zero boundary conditions: Hirota's method has been used to analyze the interaction between solitons;[13] generalized Darboux transformations (DT) have been employed to obtain rogue waves and solitons;[14] binary DT and Hirota methods have been utilized to identify soliton solutions, respectively;[15] breathers, multi-peak solitons, and the transition from breathers to solitons have been analyzed through DT;[16,17] multi-soliton solutions have been investigated via parameter modulation and asymptotic analysis.[18]

As far as we know, there have been no reports on investigations of soliton solutions for the LPDE under nonzero boundary conditions (NZBC). Thus, we investigate LPDE[19–21]

$$\begin{aligned}
&-\mathrm{i}q_{j,t}+\left[\gamma_8(t)\left[\sum_{k=1}^{2}\left(|q_k|^2\right)\right]^2-6\gamma_1(t)q_0^4\right.\\
&\left.+\zeta(t)\sum_{k=1}^{2}\left(|q_k|^2\right)-2\sigma(t)q_0^2\right]q_j+\sigma(t)q_{j,xx}\\
&+\gamma_1(t)q_{j,xxxx}+\gamma_2(t)\sum_{k=1}^{2}\left(|q_{k,x}|^2\right)q_j
\end{aligned}$$

†Corresponding author. E-mail: xiyangxie@ncepu.edu.cn

© 2024 Chinese Physical Society and IOP Publishing Ltd

$$+\gamma_3(t)\sum_{k=1}^{2}\left(q_k q_{k,x}^*\right)q_{j,x}+\gamma_4(t)\sum_{k=1}^{2}\left(q_{k,x}q_k^*\right)q_{j,x}$$
$$+\gamma_5(t)\sum_{k=1}^{2}\left(|q_k|^2\right)q_{j,xx}+\gamma_6(t)\sum_{k=1}^{2}\left(q_{k,xx}q_k^*\right)q_j$$
$$+\gamma_7(t)\sum_{k=1}^{2}\left(q_{k,xx}^*q_k\right)q_j=0,\quad (j=1,2), \tag{2}$$

with NZBC at infinity

$$\begin{cases}\lim\limits_{x\to\pm\infty}q_1=q_{1,\pm},q_{1,\pm}\in R,\\ \lim\limits_{x\to\pm\infty}q_2=q_{2,\pm},q_{2,\pm}\in R,\\ |q_{1,\pm}|^2+|q_{2,\pm}|^2=q_0^2,\quad q_0\neq 0.\end{cases}$$

Furthermore, various methods have been proposed to deal with NLS-type equations, such as the inverse scattering transform,[22–24] Lie symmetry,[25–27] DT,[28] PINN method,[29,30] Hirota bilinear method,[31] and Riemann–Hilbert (RH) methods.[32–35] The RH method is associated with the RH problem, which helps simplify the original inverse scattering transform, and it has been proved as an efficient method for solving NLS-type equations.[36–39]

However, under NZBC, the RH problem becomes more complex,[19–21] and thus only a few studies have used the RH method to explore the equations, which is the main focus of this paper. In this manuscript, we aim to reveal the characteristics of solitons, and uncover various intriguing phenomena of soliton propagations and interactions.

The frame of article is: The Lax pair and spectral for Eq. (2) are analyzed in Section 2, and the discrete spectra are characterized in Section 3. Soliton solutions are obtained in the form of an RH problem involving simple poles in Section 4. In Section 5, dynamics of the solitons are discussed and analyzed, and conclusions are addressed in Section 6.

2. Direct scattering

Equation (2) admits the Lax pair[15–18]

$$\Psi_x=X\Psi,\quad \Psi_t=T\Psi, \tag{3}$$

where

$$\begin{aligned}X&=\mathrm{i}k\omega_3+U_1,\\ T&=k^2\left[2\mathrm{i}\sigma(t)\omega_3-4\mathrm{i}\gamma_1(t)(U_{1,x}+U_1^2)\omega_3\right]-8k^3\gamma_1(t)U_1\\ &\quad-8\mathrm{i}k^4\gamma_1(t)\omega_3+\mathrm{i}\sigma(t)(U_{1,x}+U_1^2)\omega_3\\ &\quad+k\Bigg[2\sigma(t)U_1+2\gamma_1(t)U_{1,x,x}+4\gamma_1(t)U_1\sum_{k=1}^{2}|q_k|^2\\ &\quad+2\gamma_1(t)(U_1U_{1,x}-U_{1,x}U_1)\Bigg]\\ &\quad+\mathrm{i}\gamma_1(t)\Bigg[U_{1,x,x,x}\omega_3+(U_1U_{1,x,x}+U_{1,x,x}U_1)\omega_3\\ &\quad-U_{1,x}^2\omega_3+3U_{1,x}\omega_3\sum_{k=1}^{2}|q_k|^2\Bigg]\\ &\quad+\frac{3}{2}\mathrm{i}\gamma_1(t)\Bigg[U_1(I+\omega_3)\sum_{k=1}^{2}q_k^*q_{k,x}\\ &\quad+U_1(\omega_3-I)\sum_{k=1}^{2}q_kq_{k,x}^*+2U_1^2\omega_3\sum_{k=1}^{2}|q_k|^2\Bigg]\\ &\quad+\mathrm{i}\left[3q_0^4\gamma_1(t)+q_0^2\sigma(t)\right]\omega_3,\\ U_1&=\begin{pmatrix}0&q_1&q_2\\-q_1^*&0&0\\-q_2^*&0&0\end{pmatrix},\quad \omega_3=\begin{pmatrix}-1&0&0\\0&1&0\\0&0&1\end{pmatrix},\end{aligned}$$

with $\Psi(x,t,\lambda)$ denoting the eigenfunction and λ being the parameter.

We can easily prove that Eq. (2) is integrable under

$$\begin{aligned}&\zeta(t)=2\sigma(t),\quad \gamma_2(t)=2\gamma_1(t),\\ &\gamma_3(t)=2\gamma_1(t),\quad \gamma_4(t)=6\gamma_1(t),\\ &\gamma_5(t)=4\gamma_1(t),\quad \gamma_6(t)=4\gamma_1(t),\\ &\gamma_7(t)=2\gamma_1(t),\quad \gamma_8(t)=6\gamma_1(t).\end{aligned}$$

2.1. Riemann surface

Firstly, we analyze asymptotic scattering problem to derive the Jost eigenfunctions as $x\to\pm\infty$

$$\Psi_x=X_\pm\Psi,\quad \Psi_t=T_\pm\Psi, \tag{4}$$

with

$$\begin{aligned}X_\pm&=\lim_{x\to\pm\infty}X=\mathrm{i}k\omega_3+U_{1,\pm},\\ T_\pm&=\lim_{x\to\pm\infty}T=-\mathrm{i}\left(k^2+q_0^2\right)\left[\left(4k^2-3q_0^2\right)\gamma_1(t)-\sigma(t)\right]I\\ &\quad+k\left[\left(-8k^2+4q_0^2\right)\gamma_1(t)+2\sigma(t)\right]X_\pm\\ &\quad-\mathrm{i}\left[\left(4k^2-3q_0^2\right)\gamma_1(t)-\sigma(t)\right]X_\pm^2,\\ U_{1,\pm}&=\lim_{x\to\pm\infty}U_1=\begin{pmatrix}0&q_{1,\pm}&q_{2,\pm}\\-q_{1,\pm}^*&0&0\\-q_{2,\pm}^*&0&0\end{pmatrix}.\end{aligned}$$

Then we consider the transformation $z=k+\lambda$, one obtains $k=(1/2)(z+1/z)$ and $\lambda=(1/2)(z-1/z)$.

2.2. Jost solutions

Subsequently, we express the eigenvalues and the corresponding eigenvector matrices as follows:

$$\mathrm{i}J=\begin{pmatrix}-\mathrm{i}\lambda&0&0\\0&\mathrm{i}k&0\\0&0&\mathrm{i}\lambda\end{pmatrix},$$
$$E_\pm(z)=\begin{pmatrix}1&0&-\dfrac{\mathrm{i}q_0}{z}\\ \dfrac{-\mathrm{i}q_{1,\pm}^*}{z}&\dfrac{q_{2,\pm}}{q_0}&\dfrac{q_{1,\pm}^*}{q_0}\\ \dfrac{-\mathrm{i}q_{2,\pm}^*}{z}&-\dfrac{q_{1,\pm}}{q_0}&\dfrac{q_{2,\pm}^*}{q_0}\end{pmatrix}, \tag{5}$$

so that

$$X_\pm E_\pm=E_\pm\mathrm{i}J, \tag{6}$$

with $\det(E_\pm)=\eta(z)=1+q_0^2/z^2$, then we have

$$T_\pm E_\pm = E_\pm \mathrm{i}\Omega, \tag{7}$$

where

$$\mathrm{i}\Omega = \begin{pmatrix} \mathrm{i}\Omega_1 & 0 & 0 \\ 0 & \mathrm{i}\Omega_2 & 0 \\ 0 & 0 & -\mathrm{i}\Omega_1 \end{pmatrix},$$

with

$$\Omega_1 = 2k\lambda\left[\left(4k^2-2q_0^2\right)\int\gamma_1(t)\,\mathrm{d}t+\int\sigma(t)\,\mathrm{d}t\right],$$
$$\Omega_2 = \left(3q_0^4-8k^4\right)\int\gamma_1(t)\,\mathrm{d}t+\left(2k^2+q_0^2\right)\int\sigma(t)\,\mathrm{d}t.$$

Supposing that z represents the spectrum, one thus can define

$$\Psi_\pm(x,t,z) = E_\pm(z)\,\mathrm{e}^{\mathrm{i}\,\mathrm{diag}(\theta_1(x,t,z),\theta_2(x,t,z),-\theta_1(x,t,z))}+o(1),$$
$$x\to\pm\infty, \tag{8}$$

with

$$\theta_1(x,t,z) = -\lambda x+2k\lambda\left[\left(4k^2-2q_0^2\right)\int\gamma_1(t)\,\mathrm{d}t+\int\sigma(t)\,\mathrm{d}t\right],$$
$$\theta_2(x,t,z) = kx+\left(3q_0^4-8k^4\right)\int\gamma_1(t)\,\mathrm{d}t+\left(2k^2+q_0^2\right)\int\sigma(t)\,\mathrm{d}t.$$

To enhance the understanding of the definition provided above, we get

$$(\Psi_\pm)_x = X_\pm\Psi_\pm+\Delta U_{1,\pm}\Psi_\pm, \tag{9}$$

with $\Delta U_{1,\pm}=U_1-U_{1,\pm}$. Introducing the Jost eigenfunction

$$\zeta_\pm(x,t,z) = \Psi_\pm(x,t,z)\,\mathrm{e}^{-\mathrm{i}\Theta(x,t,z)}, \tag{10}$$

obviously, when $x\to\pm\infty$, we have

$$\lim_{x\to\pm\infty}\zeta_\pm(x,t,z) = E_\pm(z). \tag{11}$$

By substituting eigenfunction (10) into Lax pair (9), one has

$$\left(E_\pm^{-1}\zeta_\pm\right)_x = \mathrm{i}\left[J,E_\pm^{-1}\zeta_\pm\right]+E_\pm^{-1}\Delta U_{1,\pm}\zeta_\pm. \tag{12}$$

Then, the solutions of Lax pair (12) have the forms

$$E_-^{-1}\zeta_- = I-\int_{-\infty}^{x}\mathrm{e}^{\mathrm{i}\lambda(x-y)J(z)}E_\pm^{-1}\Delta U_{1,\pm}\zeta_\pm\,\mathrm{e}^{-\mathrm{i}\lambda(x-y)J(z)}\,\mathrm{d}y, \tag{13}$$
$$E_+^{-1}\zeta_+ = I+\int_{x}^{\infty}\mathrm{e}^{\mathrm{i}\lambda(x-y)J(z)}E_\pm^{-1}\Delta U_{1,\pm}\zeta_\pm\,\mathrm{e}^{-\mathrm{i}\lambda(x-y)J(z)}\,\mathrm{d}y. \tag{14}$$

Rewriting expressions (13) and (14) as the partitioned matrix form, we then derive

$$\zeta_\pm = \left([\zeta_\pm]_1,[\zeta_\pm]_2,[\zeta_\pm]_3\right). \tag{15}$$

$\zeta_-(x,t,z)$ or, equivalently, $\zeta_+(x,t,z)$ are extended as

$$[\zeta_-]_1 : z\in\omega_1,\quad [\zeta_-]_2 : \mathrm{Im}z<0,\quad [\zeta_-]_3 : z\in\omega_4,$$
$$[\zeta_+]_1 : z\in\omega_2,\quad [\zeta_+]_2 : \mathrm{Im}z>0,\quad [\zeta_+]_3 : z\in\omega_3, \tag{16}$$

where

$$\omega_1 = \{z:\ \mathrm{Im}z>0\wedge|z|>q_0\},$$
$$\omega_2 = \{z:\ \mathrm{Im}z<0\wedge|z|>q_0\},$$
$$\omega_3 = \{z:\ \mathrm{Im}z<0\wedge|z|<q_0\},$$
$$\omega_4 = \{z:\ \mathrm{Im}z>0\wedge|z|<q_0\}.$$

Owing to $\Psi_-(x,t,z)$ and $\Psi_+(x,t,z)$ are solutions for Eq. (3), they are linearly correlated by $A(z)$

$$\Psi_-(x,t,z) = \Psi_+(x,t,z)A(z),\ z\in\Sigma\backslash\pm\mathrm{i}q_0. \tag{17}$$

Next, $(\det\Psi)_x=\mathrm{tr}X(\det\Psi)$ and $\partial_t(\det\Psi)=\mathrm{tr}T(\det\Psi)$ can be obtained using Abel's identity. When $\mathrm{tr}X=\mathrm{i}k$ and $\mathrm{tr}T=\mathrm{i}\left(3q_0^4-8k^4\right)\int\gamma_1(t)\,\mathrm{d}t+\mathrm{i}\left(2k^2+q_0^2\right)\int\sigma(t)\,\mathrm{d}t$, we have

$$\frac{\partial}{\partial_x}\left[\Psi_\pm(x,t,z)\,\mathrm{e}^{-\mathrm{i}\Theta(x,t,z)}\right] = \frac{\partial}{\partial_t}\left[\Psi_\pm(x,t,z)\,\mathrm{e}^{-\mathrm{i}\Theta(x,t,z)}\right]=0. \tag{18}$$

Then we consider expression (8), which implies

$$\det\Psi_\pm(x,t,z) = \eta(z)\,\mathrm{e}^{\mathrm{i}\theta_2(x,t,z)},$$
$$(x,t)\in R^2,\quad z\in\Sigma\backslash\pm\mathrm{i}q_0. \tag{19}$$

Since $A(z)=(a_{ij}(z))$ is independent of t and considering expressions (17)–(19), we have

$$\det A(z)=1,\quad z\in\Sigma\backslash\pm\mathrm{i}q_0, \tag{20}$$

and $B(z)=(b_{ij}(z))=A^{-1}(z)$.

Under the assumptions as in the analysis of Eq. (16), the subsequent scattering coefficients are extended outside of Σ in

$$a_{11} : z\in\omega_1,\quad a_{22} : \mathrm{Im}z<0,\quad a_{33} : z\in\omega_4,$$
$$b_{11} : z\in\omega_2,\quad b_{22} : \mathrm{Im}z>0,\quad b_{33} : z\in\omega_3. \tag{21}$$

To formulate a scattering problem, a fully analytical function is necessary, yet $\zeta_\pm(x,t,z)$ lacks analytical properties in any region.

2.3. Adjoint problem

Considering

$$\tilde\Psi_x = (-\mathrm{i}k\omega_3+U_1^*)\tilde\Psi,\quad \tilde\Psi_t = T^*\tilde\Psi, \tag{22}$$

we have $U_1^{\mathrm{T}}=-U_1^*$, which implies $U_1^\dagger=-U_1$.

If $\tilde v$ and $\tilde w$ are the solutions for Eq. (22), then we have

$$u(x,t,z) = \mathrm{e}^{\mathrm{i}\theta_2(x,t,z)}\left[\tilde v\times\tilde w\right](x,t,z), \tag{23}$$

which constitutes the solution for the original Lax pair (3).

Next, we obtain

$$\tilde{\Psi}_x(x,t,z)=\tilde{E}_{\pm}(x,t,z)\,\mathrm{e}^{-\mathrm{i}\Theta(x,t,z)}+o(1),\quad x\to\pm\infty. \tag{24}$$

With $\tilde{\zeta}_{\pm}(x,t,z)=\tilde{\Psi}_{\pm}(x,t,z)\,\mathrm{e}^{-\mathrm{i}\Theta(x,t,z)}$ as previously defined, it is demonstrated that $\tilde{\zeta}_{\pm}(x,t,z)=\left([\tilde{\zeta}_{\pm}]_1,[\tilde{\zeta}_{\pm}]_2,[\tilde{\zeta}_{\pm}]_3\right)$ are extended as

$$\begin{aligned}&[\tilde{\zeta}_-]_1:z\in D_2,\quad [\tilde{\zeta}_-]_2:\mathrm{Im}z>0,\quad [\tilde{\zeta}_-]_3:z\in D_3,\\&[\tilde{\zeta}_+]_1:z\in D_1,\quad [\tilde{\zeta}_+]_2:\mathrm{Im}z<0,\quad [\tilde{\zeta}_+]_3:z\in D_4.\end{aligned} \tag{25}$$

Similar to before, given that $\tilde{\Psi}_{\pm}(x,t,z)$, we have

$$\tilde{\Psi}_-(x,t,z)=\tilde{\Psi}_+(x,t,z)\tilde{A}(z),\quad \tilde{B}(z)=\tilde{A}^{-1}(z). \tag{26}$$

From this relationship, we can introduce $\tilde{A}(z)=(\tilde{a}_{ij}(z))$ and $\tilde{B}(z)=(\tilde{b}_{ij}(z))$ as

$$\begin{aligned}&\tilde{a}_{11}:\ z\in\omega_2,\quad \tilde{a}_{22}:\ \mathrm{Im}z>0,\quad \tilde{a}_{33}:\ z\in\omega_3,\\&\tilde{b}_{11}:\ z\in\omega_1,\quad \tilde{b}_{22}:\ \mathrm{Im}z<0,\quad \tilde{b}_{33}:\ z\in\omega_4.\end{aligned} \tag{27}$$

In the end, one gets the new solutions as

$$\begin{aligned}\Psi_1(x,t,z)&=\mathrm{e}^{\mathrm{i}\theta_2(x,t,z)}\left[\tilde{\Psi}_{+,1}\times\tilde{\Psi}_{-,2}\right](x,t,z),\\\Psi_2(x,t,z)&=\mathrm{e}^{\mathrm{i}\theta_2(x,t,z)}\left[\tilde{\Psi}_{-,1}\times\tilde{\Psi}_{+,2}\right](x,t,z),\\\Psi_3(x,t,z)&=\mathrm{e}^{\mathrm{i}\theta_2(x,t,z)}\left[\tilde{\Psi}_{+,2}\times\tilde{\Psi}_{-,3}\right](x,t,z),\\\Psi_4(x,t,z)&=\mathrm{e}^{\mathrm{i}\theta_2(x,t,z)}\left[\tilde{\Psi}_{-,2}\times\tilde{\Psi}_{+,3}\right](x,t,z),\end{aligned} \tag{28}$$

where Ψ_j's are analytic. In the focusing scenario, there exist four distinct domains ω_j $(j=1,2,3,4)$ of analyticity.

As $z\in\Sigma$, one has

$$\begin{aligned}\Psi_{\pm,i}(x,t,z)&=\frac{\mathrm{e}^{\mathrm{i}\theta_2(x,t,z)}[\tilde{\Psi}_{\pm,j}\times\tilde{\Psi}_{\pm,m}](x,t,z)}{\xi_j(z)},\\\tilde{\Psi}_{\pm,i}(x,t,z)&=\frac{\mathrm{e}^{-\mathrm{i}\theta_2(x,t,z)}\left[\Psi_{\pm,j}\times\Psi_{\pm,m}\right](x,t,z)}{\xi_j(z)},\end{aligned} \tag{29}$$

where

$$\xi(z)=\mathrm{diag}(\xi_1,\xi_2,\xi_3),\ \xi_1=\xi_3=1,\ \xi_2=\eta(z).$$

Obviously, we obtain the relationship as

$$\tilde{A}(z)=\xi(z)(A^{-1}(z))^{\mathrm{T}}\xi^{-1}(z). \tag{30}$$

Moreover, it is beneficial to eliminate the oscillations, so we introduce

$$\begin{aligned}\tau_j(x,t,z)&=\Psi_j(x,t,z)\,\mathrm{e}^{\mathrm{i}\theta_1(x,t,z)},\ j=1,2,\\\tau_j(x,t,z)&=\Psi_j(x,t,z)\,\mathrm{e}^{-\mathrm{i}\theta_1(x,t,z)},\ j=3,4.\end{aligned} \tag{31}$$

2.4. Symmetries

In the case of LPDE under ZBC, the sole symmetry is $k\to k^*$. However, the symmetries become more intricate with NZBC, and one of these symmetries mirrors that of the ZBC case. Additionally, the symmetries under NZBC are further complex since the Jost solutions do not converge to I. It is worth noting that $z=k+\lambda$ and $\hat{z}=k-\lambda$.

(i) The first symmetry: Consider $z\to z^*$, which implies $(k,\lambda)\to(k^*,\lambda^*)$. The Jost eigenfunctions satisfy

$$(\Psi_{\pm}^{\dagger}(x,t,z^*))^{-1}C(z)=\Psi_{\pm}(x,t,z), \tag{32}$$

with

$$C(z)=\mathrm{diag}\left(\eta(z),\ 1,\ \eta(z)\right).$$

Furthermore, by combining symmetry relation (32) with the scattering relation (17), we obtain that

$$A^{\dagger}(z^*)=C(z)B(z)C^{-1}(z). \tag{33}$$

In addition, we have

$$\Psi^*_{\pm,i}(x,t,z^*)=\frac{\mathrm{e}^{-\mathrm{i}\theta_2(x,t,z)}[\Psi_{\pm,j}\times\Psi_{\pm,m}](x,t,z)}{\xi_j(z)}, \tag{34}$$

with i, j, and m being cyclic indices.

(ii) The second symmetry: Consider that $z\to\hat{z}$ means $(k,\lambda)\to(k,-\lambda)$, it is demonstrated that

$$\Psi_{\pm}(x,t,z)=\Psi_{\pm}(x,t,\hat{z})Q(z), \tag{35}$$

where

$$Q(z)=\begin{pmatrix}0&0&-\mathrm{i}q_0/z\\0&1&0\\-\mathrm{i}q_0/z&0&0\end{pmatrix}.$$

Then, we can demonstrate that

$$A(\hat{z})=Q(z)B(z)Q^{-1}(z),\quad z\in\Sigma. \tag{36}$$

3. Asymptotic behavior

3.1. Discrete spectrum

The discrete spectra for the focused Manakov equations under NZBC exhibit complex structure compared to those of the focused case with ZBC. For depicting the discrete spectrum, one derives

$$\begin{aligned}P_1(x,t,z)&=(\Psi_{-,1},\ \Psi_{+,2},\ \Psi_1)(x,t,z),\ z\in D_1,\\P_2(x,t,z)&=(\Psi_{+,1},\ \Psi_{-,2},\ \Psi_2)(x,t,z),\ z\in D_2,\\P_3(x,t,z)&=(\Psi_3,\ \Psi_{-,2},\ \Psi_{+,3})(x,t,z),\ z\in D_3,\\P_4(x,t,z)&=(\Psi_4,\ \Psi_{+,2},\ \Psi_{-,3})(x,t,z),\ z\in D_4.\end{aligned} \tag{37}$$

Referring to symmetry relations (32), we get

$$\begin{aligned}\mathrm{Wr}P_1(x,t,z)&=a_{11}(z)b_{22}(z)\,\mathrm{e}^{\mathrm{i}\theta_2(x,t,z)},\\\mathrm{Wr}P_2(x,t,z)&=a_{22}(z)b_{11}(z)\,\mathrm{e}^{\mathrm{i}\theta_2(x,t,z)},\\\mathrm{Wr}P_3(x,t,z)&=a_{22}(z)b_{33}(z)\,\mathrm{e}^{\mathrm{i}\theta_2(x,t,z)},\\\mathrm{Wr}P_4(x,t,z)&=a_{33}(z)b_{22}(z)\,\mathrm{e}^{\mathrm{i}\theta_2(x,t,z)}.\end{aligned} \tag{38}$$

When $\mathrm{Im}\lambda > 0$, the following equivalences hold:

$$\begin{aligned} &b_{22}(z_0) = 0 \Leftrightarrow a_{22}(z_0^*) = 0 \Leftrightarrow \\ &a_{22}(\hat{z}_0^*) = 0 \Leftrightarrow b_{22}(\hat{z}_0) = 0, \end{aligned} \tag{39}$$

and for $\mathrm{Im}\lambda > 0$ and $|z_0| \geq q_0$, one obtains

$$\begin{aligned} &a_{11}(z_0) = 0 \Leftrightarrow b_{11}(z_0^*) = 0 \Leftrightarrow \\ &b_{33}(\hat{z}_0^*) = 0 \Leftrightarrow a_{33}(\hat{z}_0) = 0. \end{aligned} \tag{40}$$

Three potential types of eigenvalue quartets associated with $z_0 \in D_1$ have the forms of

$$\begin{aligned} &a_{11}(z_0) = 0 \text{ and } b_{22}(z_0) \neq 0, \\ &a_{11}(z_0) \neq 0 \text{ and } b_{22}(z_0) = 0, \\ &a_{11}(z_0) = b_{22}(z_0) = 0. \end{aligned} \tag{41}$$

If we set $z_0 \in D_1$ as a discrete eigenvalue, then the following cases hold:

(i) If z_0 belongs to the first kind, we get

$$\begin{aligned} &\Psi_{-,1}(x,t,z_0) = s_0 \frac{\Psi_1(x,t,z_0)}{b_{22}(z_0)}, \\ &\Psi_2(x,t,z_0^*) = \hat{s}_0 \Psi_{+,1}(x,t,z_0^*), \\ &\Psi_3(x,t,\hat{z}_0^*) = \check{s}_0 \Psi_{+,3}(x,t,\hat{z}_0^*), \\ &\Psi_{-,3}(x,t,\hat{z}_0) = \bar{s}_0 \Psi_4(x,t,\hat{z}_0). \end{aligned} \tag{42}$$

where s_0, $\hat{s}_0$, $\check{s}_0$, and $\bar{s}_0$ are constants.

(ii) If z_0 belongs to the second kind, we have

$$\begin{aligned} &\Psi_1(x,t,z_0) = f_0 \Psi_{+,2}(x,t,z_0), \\ &\Psi_{-,2}(x,t,z_0^*) = \hat{f}_0 \Psi_2(x,t,z_0^*), \\ &\Psi_{-,2}(x,t,\hat{z}_0^*) = \check{f}_0 \Psi_3(x,t,\hat{z}_0^*), \\ &\Psi_4(x,t,\hat{z}_0) = \bar{f}_0 \Psi_{+,2}(x,t,\hat{z}_0). \end{aligned} \tag{43}$$

with f_0, $\hat{f}_0$, $\check{f}_0$, and $\bar{f}_0$ being constants.

(iii) If z_0 belongs to the third kind, such that $\Psi_1(x,t,z_0) = \Psi_2(x,t,z_0^*) = 0$, we get

$$\begin{aligned} &\Psi_1(x,t,z_0) = n_0 \Psi_{+,2}(x,t,z_0), \\ &\Psi_{-,2}(x,t,z_0^*) = \hat{n}_0 \Psi_{+,1}(x,t,z_0^*), \\ &\Psi_{-,2}(x,t,\hat{z}_0^*) = \check{n}_0 \Psi_{+,3}(x,t,\hat{z}_0^*), \\ &\Psi_{-,3}(x,t,\hat{z}_0) = \bar{n}_0 \Psi_{+,2}(x,t,\hat{z}_0). \end{aligned} \tag{44}$$

where n_0, $\hat{n}_0$, $\check{n}_0$, and $\bar{n}_0$ are constants.

3.2. Symmetries

Next, we restate relations (42), (43), and (44) based on the modified eigenfunctions.

If $\{w_n\}_{n=1}^{N_1}$ are the eigenvalues for the first species, we get

$$\begin{aligned} &\zeta_{-,1}(x,t,w_n) = \frac{s_n}{b_{22}(w_n)} \tau_1(x,t,w_n) \mathrm{e}^{-2\mathrm{i}\theta_1(x,t,w_n)}, \\ &\tau_2(x,t,w_n^*) = \hat{s}_n \zeta_{+,1}(x,t,w_n^*) \mathrm{e}^{2\mathrm{i}\theta_1(x,t,w_n^*)}, \\ &\tau_3(x,t,\hat{w}_n^*) = \check{s}_n \zeta_{+,3}(x,t,\hat{w}_n^*) \mathrm{e}^{2\mathrm{i}\theta_1(x,t,w_n^*)}, \\ &\zeta_{-,3}(x,t,\hat{w}_n) = \bar{s}_n \tau_4(x,t,\hat{w}_n) \mathrm{e}^{-2\mathrm{i}\theta_1(x,t,w_n)}, \end{aligned} \tag{45}$$

and $\{z_n\}_{n=1}^{N_2}$ are the eigenvalues for the second species, we get

$$\begin{aligned} &\tau_1(x,t,z_n) = f_n \zeta_{+,2}(x,t,z_n) \mathrm{e}^{\mathrm{i}(\theta_1+\theta_2)(x,t,z_n)}, \\ &\zeta_{-,2}(x,t,z_n^*) = \hat{f}_n \tau_2(x,t,z_n^*) \mathrm{e}^{-\mathrm{i}(\theta_1+\theta_2)(x,t,z_n^*)}, \\ &\zeta_{-,2}(x,t,\hat{z}_n^*) = \check{f}_n \tau_2(x,t,\hat{z}_n^*) \mathrm{e}^{-\mathrm{i}(\theta_1+\theta_2)(x,t,z_n^*)}, \\ &\tau_4(x,t,\hat{z}_n) = \bar{f}_n \zeta_{+,2}(x,t,\hat{z}_n) \mathrm{e}^{\mathrm{i}(\theta_1+\theta_2)(x,t,z_n)}, \end{aligned} \tag{46}$$

while $\{\xi_n\}_{n=1}^{N_3}$ be the eigenvalues of the third species, we get

$$\begin{aligned} &\zeta_{-,1}(x,t,\xi_n) = n_n \zeta_{+,2}(x,t,\xi_n) \mathrm{e}^{-\mathrm{i}(\theta_1-\theta_2)(x,t,\xi_n)}, \\ &\zeta_{-,2}(x,t,\xi_n^*) = \hat{n}_n \zeta_{+,1}(x,t,\xi_n^*) \mathrm{e}^{\mathrm{i}(\theta_1-\theta_2)(x,t,\xi_n^*)}, \\ &\zeta_{-,2}(x,t,\xi_n^*) = \check{n}_n \zeta_{+,3}(x,t,\xi_n^*) \mathrm{e}^{\mathrm{i}(\theta_1-\theta_2)(x,t,\xi_n^*)}, \\ &\zeta_{-,3}(x,t,\hat{\xi}_n) = \bar{n}_n \zeta_{+,2}(x,t,\hat{\xi}_n) \mathrm{e}^{-\mathrm{i}(\theta_1-\theta_2)(x,t,\xi_n)}. \end{aligned} \tag{47}$$

The combination of these symmetries reveals that

$$\begin{aligned} &\bar{s}_n = \frac{s_n}{b_{22}(w_n)}, \quad \hat{s}_n = \check{s}_n = -s_n^*, \\ &\bar{f}_n = -\frac{\mathrm{i}z_n}{q_0} f_n, \quad \hat{f}_n = -\frac{f_n^*}{\eta(z_n^*) b_{11}(z_n^*)}, \\ &\check{f}_n = -\frac{\mathrm{i}q_0}{z_n^*} \frac{f_n^*}{\eta(z_n^*) b_{11}(z_n^*)}, \\ &\bar{n}_n = -\frac{\mathrm{i}\xi_n}{q_0} n_n, \quad \hat{n}_n = -\frac{a_{22}'(\xi_n^*)}{b_{11}'(\xi_n^*)} \frac{n_n^*}{\eta(\xi_n^*)}, \\ &\check{n}_n = -\frac{\mathrm{i}q_0}{\xi_n^*} \frac{a_{22}'(\xi_n^*)}{b_{11}'(\xi_n^*)} \frac{n_n^*}{\eta(\xi_n^*)}. \end{aligned} \tag{48}$$

3.3. Asymptotic behavior

To illustrate the RH problem, we expand $\zeta_+(x,t,z)$ as

$$\zeta_+(x,t,z) = \sum_{n=0}^{\infty} \zeta_n(x,t,z), \tag{49}$$

with

$$\zeta_0(x,t,z) = E_+(z), \tag{50}$$

$$\begin{aligned} \zeta_{n+1}(x,t,z) = &-\int_{-\infty}^{x} E_+(z) \mathrm{e}^{\mathrm{i}(x-y)J(z)} E_+^{-1}(z) \\ &\times \Delta U_{1,\pm}(y,t) \zeta_n(y,t,z) \mathrm{e}^{-\mathrm{i}(x-y)J(z)} \mathrm{d}y. \end{aligned} \tag{51}$$

For all $m \geq 0$, $\zeta_+(x,t,z)$ are expanded as $z \to \infty$

$$\begin{aligned} &[\zeta_{2m}]_{\mathrm{bd}} = O\left(\frac{1}{z^m}\right), \quad [\zeta_{2m}]_{\mathrm{bo}} = O\left(\frac{1}{z^{m+1}}\right), \\ &[\zeta_{2m+1}]_{\mathrm{bd}} = O\left(\frac{1}{z^{m+1}}\right), \quad [\zeta_{2m+1}]_{\mathrm{bo}} = O\left(\frac{1}{z^{m+1}}\right). \end{aligned} \tag{52}$$

Similarly, as $z \to 0$, we obtain

$$[\zeta_{2m}]_{\mathrm{bd}} = O(z^m), \quad [\zeta_{2m}]_{\mathrm{bo}} = O(z^{m-1}), \tag{53}$$

$$[\zeta_{2m+1}]_{\mathrm{bd}} = O(z^m), \quad [\zeta_{2m+1}]_{\mathrm{bo}} = O(z^m). \tag{54}$$

When analyzing the asymptotic behavior of the block matrices in Eq. (15) as $z \to \infty$ or $z \to 0$, we analyze each limit separately.

As $z\to\infty$, we derive

$$[\zeta_\pm]_1(x,t,z)=\begin{pmatrix}1\\ -\dfrac{\mathrm{i}}{z}\boldsymbol{q}^*(x,t)\end{pmatrix}+O\left(\frac{1}{z^2}\right),$$
$$[\zeta_\pm]_2(x,t,z)=\begin{pmatrix}\dfrac{\mathrm{i}}{zq_0}\boldsymbol{q}^{\mathrm{T}}(x,t)\boldsymbol{r}_\pm^*\\ \dfrac{1}{q_0}\boldsymbol{r}_\pm^*\end{pmatrix}+O\left(\frac{1}{z^2}\right),$$
$$[\zeta_\pm]_3(x,t,z)=\begin{pmatrix}-\dfrac{\mathrm{i}}{zq_0}\boldsymbol{q}^{\mathrm{T}}(x,t)\boldsymbol{q}_\pm^*\\ \dfrac{1}{q_0}\boldsymbol{q}_\pm^*\end{pmatrix}+O\left(\frac{1}{z^2}\right),\tag{55}$$

where $\boldsymbol{q}(x,t)=(q_1(x,t),q_2(x,t))^{\mathrm{T}}$, $\boldsymbol{r}_\pm=(q_{2,\pm},-q_{1,\pm})^\dagger$, and $\boldsymbol{q}_\pm=(q_{1,\pm},q_{2,\pm})^{\mathrm{T}}$.

Similarly, as $z\to 0$, one obtains

$$[\zeta_\pm]_1(x,t,z)=\begin{pmatrix}\dfrac{1}{q_0^2}\boldsymbol{q}^{\mathrm{T}}(x,t)\boldsymbol{q}_\pm^*\\ -\dfrac{\mathrm{i}}{z}\boldsymbol{q}_\pm^*\end{pmatrix}+O(z),$$
$$[\zeta_\pm]_2(x,t,z)=\begin{pmatrix}0\\ \dfrac{1}{q_0}\boldsymbol{r}_\pm^*\end{pmatrix}+O(z),$$
$$[\zeta_\pm]_3(x,t,z)=\begin{pmatrix}-\dfrac{\mathrm{i}q_0}{z}\\ \dfrac{1}{q_0}\boldsymbol{q}^*(x,t)\end{pmatrix}+O(z).\tag{56}$$

To simplify the analysis, we eliminate their exponential oscillations by considering the modified auxiliary eigenfunctions defined in expression (31).

Summarizing the above relations, we derive

(i) $z\to\infty$

$$a_{11}(z)=1+O\left(\frac{1}{z}\right),\quad a_{22}(z)=\frac{1}{q_0^2}\boldsymbol{q}_-^{\mathrm{T}}\boldsymbol{q}_+^*+O\left(\frac{1}{z}\right),$$
$$a_{33}(z)=\frac{1}{q_0^2}\boldsymbol{q}_+^{\mathrm{T}}\boldsymbol{q}_-^*+O\left(\frac{1}{z}\right),$$
$$b_{11}(z)=1+O\left(\frac{1}{z}\right),\quad b_{22}(z)=\frac{1}{q_0^2}\boldsymbol{q}_+^{\mathrm{T}}\boldsymbol{q}_-^*+O\left(\frac{1}{z}\right),$$
$$b_{33}(z)=\frac{1}{q_0^2}\boldsymbol{q}_-^{\mathrm{T}}\boldsymbol{q}_+^*+O\left(\frac{1}{z}\right).\tag{57}$$

(ii) $z\to 0$

$$a_{11}(z)=\frac{1}{q_0^2}\boldsymbol{q}_+^{\mathrm{T}}\boldsymbol{q}_-^*+O(z),\quad a_{22}(z)=\frac{1}{q_0^2}\boldsymbol{q}_-^{\mathrm{T}}\boldsymbol{q}_+^*+O(z),$$
$$a_{33}(z)=1+O(z),$$
$$b_{11}(z)=\frac{1}{q_0^2}\boldsymbol{q}_-^{\mathrm{T}}\boldsymbol{q}_+^*+O(z),\quad b_{22}(z)=\frac{1}{q_0^2}\boldsymbol{q}_+^{\mathrm{T}}\boldsymbol{q}_-^*+O(z),$$
$$b_{33}(z)=1+O(z).\tag{58}$$

4. Riemann–Hilbert problem (RHP)

4.1. Generalized RHP

Setting $M_j(x,t,z)$ as

$$M_1(x,t,z)=P_1\,\mathrm{e}^{-\mathrm{i}\Theta}\,[\mathrm{diag}(a_{11},1,b_{22})]^{-1}$$
$$=\begin{pmatrix}\dfrac{\zeta_{-,1}}{a_{11}} & \zeta_{+,2} & \dfrac{\tau_1}{b_{22}}\end{pmatrix},\quad z\in D_1,\tag{59}$$
$$M_2(x,t,z)=P_2\,\mathrm{e}^{-\mathrm{i}\Theta}\,[\mathrm{diag}(1,a_{22},b_{11})]^{-1}$$
$$=\begin{pmatrix}\zeta_{+,1} & \dfrac{\zeta_{-,2}}{a_{22}} & \dfrac{\tau_2}{b_{11}}\end{pmatrix},\quad z\in D_2,\tag{60}$$
$$M_3(x,t,z)=P_3\,\mathrm{e}^{-\mathrm{i}\Theta}\,[\mathrm{diag}(a_{11},1,b_{22})]^{-1}$$
$$=\begin{pmatrix}\dfrac{\tau_3}{b_{33}} & \dfrac{\zeta_{-,2}}{a_{22}} & \zeta_{+,3}\end{pmatrix},\quad z\in D_3,\tag{61}$$
$$M_4(x,t,z)=P_4\,\mathrm{e}^{-\mathrm{i}\Theta}\,[\mathrm{diag}(b_{22},1,a_{33})]^{-1}$$
$$=\begin{pmatrix}\dfrac{\tau_4}{b_{22}} & \zeta_{+,2} & \dfrac{\zeta_{-,3}}{a_{33}}\end{pmatrix},\quad z\in D_4,\tag{62}$$

then, $M_j(x,t,z)$s obey

$$M^+(x,t,z)=M^-(x,t,z)\left[I-\mathrm{e}^{\mathrm{i}\Theta(x,t,z)}L(z)\,\mathrm{e}^{-\mathrm{i}\Theta(x,t,z)}\right],$$
$$z\in\Sigma,\tag{63}$$

with $M=M^+$ for $z\in D^+$ and $M=M^-$ for $z\in D^-$. $L(x,t,z)$ is defined on each segment Σ_j $(j=1,2,3,4)$ of the contour as follows:

$$L(x,t,z)=\begin{pmatrix}\dfrac{\mathrm{i}q_0}{z}\rho_1\hat\rho_3-R_2-\rho_1R_2\rho_3 & \dfrac{\mathrm{i}q_0}{z}\hat\rho_3+R_2\rho_3 & -R_2-\dfrac{\mathrm{i}q_0}{z}\eta\hat\rho_3R_3-\eta R_2\rho_3R_3\\ -\rho_1 & 0 & \eta R_3\\ -\rho_1-\rho_2 & \rho_3 & -\eta\rho_3R_3\end{pmatrix},\quad z\in\Sigma_1,\tag{64}$$

$$L(x,t,z)=\begin{pmatrix}\hat R_2R_2 & 0 & -R_2\\ 0 & 0 & 0\\ \hat R_2 & 0 & 0\end{pmatrix},\quad z\in\Sigma_2,\tag{65}$$

$$L(x,t,z)=\begin{pmatrix}-\hat\rho_1\hat R_2 & \hat\rho_2\rho_3-\dfrac{\mathrm{i}q_0}{z}\hat\rho_3 & \hat\rho_2\\ \dfrac{\mathrm{i}z}{q_0}\hat\rho_1\hat R_2-\dfrac{\mathrm{i}z}{q_0}\eta\hat R_3-\eta\hat\rho_2\hat R_2R_3 & \eta(\hat\rho_3\hat R_3+\hat\rho_2\rho_3R_3) & \eta\hat\rho_2R_3\\ \hat R_2 & -\rho_3 & 0\end{pmatrix},\quad z\in\Sigma_3,\tag{66}$$

$$L(x,t,z)=\begin{pmatrix} \rho_2\hat{\rho}_2 & 0 & \hat{\rho}_2 \\ \dfrac{\mathrm{i}q_0\eta}{z}\hat{R}_3(1-\rho_2\hat{\rho}_2)-\rho_1+\dfrac{\mathrm{i}z}{q_0}\hat{\rho}_1\rho_2 & \eta & \eta(\rho_3-\dfrac{\mathrm{i}q_0}{z}\hat{\rho}_2\hat{R}_3)-\dfrac{\mathrm{i}z}{q_0}\hat{\rho}_1 \\ -\hat{\rho}_2 & 0 & 0 \end{pmatrix}, \quad z\in\Sigma_4, \tag{67}$$

with $\rho_j=\rho_j(z)$ and $R_j=\rho_j^*(z^*)$.

To ensure the uniqueness of the RHP (63), an appropriate normalization condition must be specified. Then, we obtain the following expressions:

$$M(x,t,z)=M_\infty+O\left(\frac{1}{z}\right), \quad z\to\infty, \tag{68}$$

$$M(x,t,z)=\frac{\mathrm{i}}{z}M_0+O(1), \quad z\to 0, \tag{69}$$

with

$$M_\infty=\begin{pmatrix} 1 & 0 & 0 \\ 0 & \dfrac{1}{q_0}\boldsymbol{r}_+ & \dfrac{1}{q_0}\boldsymbol{q}_+ \end{pmatrix} \quad \text{and} \quad M_0=\begin{pmatrix} 0 & 0 & q_0 \\ \boldsymbol{q}_+ & \mathbf{0} & \mathbf{0} \end{pmatrix}.$$

Setting the residue of $M^{\pm}_{-1,w}(x,t)$ by $M^{\pm}$, with $M^{\pm}=(\tau_1^{\pm},\tau_2^{\pm},\tau_3^{\pm})$, then we have

$$\begin{aligned} &M^{+}_{-1,w_n}(x,t)=S_n(\tau_3^{+}(w_n),\mathbf{0},\mathbf{0}),\\ &M^{-}_{-1,w_n^*}(x,t)=\hat{S}_n(\mathbf{0},\mathbf{0},\tau_1^{-}(w_n^*)), \end{aligned} \tag{70}$$

$$\begin{aligned} &M^{+}_{-1,\hat{w}_n^*}(x,t)=-\frac{\mathrm{i}w_n^*}{q_0}\check{S}_n(\tau_1^{-}(w_n^*),\mathbf{0},\mathbf{0}),\\ &M^{-}_{-1,\hat{w}_n}(x,t)=-\frac{\mathrm{i}w_n}{q_0}\bar{S}_n(\mathbf{0},\mathbf{0},\tau_3^{+}(w_n)), \end{aligned} \tag{71}$$

$$\begin{aligned} &M^{+}_{-1,z_n}(x,t)=F_n(\mathbf{0},\mathbf{0},\tau_2^{+}(z_n)),\\ &M^{-}_{-1,z_n^*}(x,t)=\hat{F}_n(\mathbf{0},\tau_3^{-}(z_n^*),\mathbf{0}), \end{aligned} \tag{72}$$

$$\begin{aligned} &M^{+}_{-1,\hat{z}_n^*}(x,t)=-\frac{\mathrm{i}z_n^*}{q_0}\check{F}_n(\mathbf{0},\tau_3^{-}(z_n^*),\mathbf{0}),\\ &M^{-}_{-1,\hat{z}_n}(x,t)=\bar{F}_n(\tau_2^{+}(z_n),\mathbf{0},\mathbf{0}), \end{aligned} \tag{73}$$

$$\begin{aligned} &M^{+}_{-1,\xi_n}(x,t)=N_n(\tau_2^{+}(\xi_n),\mathbf{0},\mathbf{0}),\\ &M^{-}_{-1,\xi_n^*}(x,t)=\hat{N}_n(\mathbf{0},\tau_1^{-}(\xi_n^*),\mathbf{0}), \end{aligned} \tag{74}$$

$$\begin{aligned} &M^{+}_{-1,\xi_n}(x,t)=-\frac{\mathrm{i}\xi_n^*}{q_0}\check{N}_n(\mathbf{0},\tau_1^{-}(\xi_n^*),\mathbf{0}),\\ &M^{-}_{-1,\hat{\xi}_n}(x,t)=\bar{N}_n(\mathbf{0},\mathbf{0},\tau_2^{+}(\xi_n)), \end{aligned} \tag{75}$$

with

$$\begin{aligned} S_n(x,t)&=\frac{s_n}{a_{11}'(w_n)}\mathrm{e}^{-2\mathrm{i}\theta_1(w_n)},\\ \hat{S}_n(x,t)&=\frac{\hat{s}_n}{b_{11}'(w_n^*)}\mathrm{e}^{2\mathrm{i}\theta_1(w_n^*)},\\ \check{S}_n(x,t)&=\frac{\check{s}_n}{b_{33}'(\hat{w}_n^*)}\mathrm{e}^{2\mathrm{i}\theta_1(w_n^*)},\\ \bar{S}_n(x,t)&=\frac{\bar{s}_n b_{22}(w_n)}{a_{33}'(\hat{w}_n)}\mathrm{e}^{-2\mathrm{i}\theta_1(w_n)},\\ F_n(x,t)&=\frac{f_n}{b_{22}'(z_n)}\mathrm{e}^{\mathrm{i}(\theta_1+\theta_2)(z_n)},\\ \hat{F}_n(x,t)&=\frac{\hat{f}_n b_{11}(z_n^*)}{a_{22}'(z_n^*)}\mathrm{e}^{-\mathrm{i}(\theta_1+\theta_2)(z_n^*)}, \end{aligned} \tag{76}$$

$$\begin{aligned} \check{F}_n(x,t)&=\frac{\check{f}_n b_{11}(z_n^*)}{a_{22}'(\hat{z}_n^*)}\mathrm{e}^{-\mathrm{i}(\theta_1+\theta_2)(z_n^*)},\\ \bar{F}_n(x,t)&=\frac{\bar{f}_n}{a_{22}'(\hat{z}_n)}\mathrm{e}^{\mathrm{i}(\theta_1+\theta_2)(z_n)},\\ N_n(x,t)&=\frac{n_n}{a_{11}'(\xi_n)}\mathrm{e}^{-\mathrm{i}(\theta_1-\theta_2)(\xi_n)},\\ \hat{N}_n(x,t)&=\frac{\hat{n}_n}{a_{22}'(\xi_n^*)}\mathrm{e}^{\mathrm{i}(\theta_1-\theta_2)(\xi_n^*)},\\ \check{N}_n(x,t)&=\frac{\check{n}_n}{a_{22}'(\hat{\xi}_n^*)}\mathrm{e}^{\mathrm{i}(\theta_1-\theta_2)(\xi_n^*)},\\ \bar{N}_n(x,t)&=\frac{\bar{n}_n}{a_{33}'(\hat{\xi}_n)}\mathrm{e}^{-\mathrm{i}(\theta_1-\theta_2)(\xi_n)}. \end{aligned} \tag{77}$$

$$\begin{aligned} \check{F}_n(x,t)&=\frac{\check{f}_n b_{11}(z_n^*)}{a_{22}'(\hat{z}_n^*)}\mathrm{e}^{-\mathrm{i}(\theta_1+\theta_2)(z_n^*)},\\ \bar{F}_n(x,t)&=\frac{\bar{f}_n}{a_{22}'(\hat{z}_n)}\mathrm{e}^{\mathrm{i}(\theta_1+\theta_2)(z_n)},\\ N_n(x,t)&=\frac{n_n}{a_{11}'(\xi_n)}\mathrm{e}^{-\mathrm{i}(\theta_1-\theta_2)(\xi_n)},\\ \hat{N}_n(x,t)&=\frac{\hat{n}_n}{a_{22}'(\xi_n^*)}\mathrm{e}^{\mathrm{i}(\theta_1-\theta_2)(\xi_n^*)},\\ \check{N}_n(x,t)&=\frac{\check{n}_n}{a_{22}'(\hat{\xi}_n^*)}\mathrm{e}^{\mathrm{i}(\theta_1-\theta_2)(\xi_n^*)},\\ \bar{N}_n(x,t)&=\frac{\bar{n}_n}{a_{33}'(\hat{\xi}_n)}\mathrm{e}^{-\mathrm{i}(\theta_1-\theta_2)(\xi_n)}. \end{aligned} \tag{78}$$

$$\begin{aligned} \check{F}_n(x,t)&=\frac{\check{f}_n b_{11}(z_n^*)}{a_{22}'(\hat{z}_n^*)}\mathrm{e}^{-\mathrm{i}(\theta_1+\theta_2)(z_n^*)},\\ \bar{F}_n(x,t)&=\frac{\bar{f}_n}{a_{22}'(\hat{z}_n)}\mathrm{e}^{\mathrm{i}(\theta_1+\theta_2)(z_n)},\\ N_n(x,t)&=\frac{n_n}{a_{11}'(\xi_n)}\mathrm{e}^{-\mathrm{i}(\theta_1-\theta_2)(\xi_n)},\\ \hat{N}_n(x,t)&=\frac{\hat{n}_n}{a_{22}'(\xi_n^*)}\mathrm{e}^{\mathrm{i}(\theta_1-\theta_2)(\xi_n^*)},\\ \check{N}_n(x,t)&=\frac{\check{n}_n}{a_{22}'(\hat{\xi}_n^*)}\mathrm{e}^{\mathrm{i}(\theta_1-\theta_2)(\xi_n^*)},\\ \bar{N}_n(x,t)&=\frac{\bar{n}_n}{a_{33}'(\hat{\xi}_n)}\mathrm{e}^{-\mathrm{i}(\theta_1-\theta_2)(\xi_n)}. \end{aligned} \tag{79}$$

$$\begin{aligned} \check{F}_n(x,t)&=\frac{\check{f}_n b_{11}(z_n^*)}{a_{22}'(\hat{z}_n^*)}\mathrm{e}^{-\mathrm{i}(\theta_1+\theta_2)(z_n^*)},\\ \bar{F}_n(x,t)&=\frac{\bar{f}_n}{a_{22}'(\hat{z}_n)}\mathrm{e}^{\mathrm{i}(\theta_1+\theta_2)(z_n)},\\ N_n(x,t)&=\frac{n_n}{a_{11}'(\xi_n)}\mathrm{e}^{-\mathrm{i}(\theta_1-\theta_2)(\xi_n)},\\ \hat{N}_n(x,t)&=\frac{\hat{n}_n}{a_{22}'(\xi_n^*)}\mathrm{e}^{\mathrm{i}(\theta_1-\theta_2)(\xi_n^*)},\\ \check{N}_n(x,t)&=\frac{\check{n}_n}{a_{22}'(\hat{\xi}_n^*)}\mathrm{e}^{\mathrm{i}(\theta_1-\theta_2)(\xi_n^*)},\\ \bar{N}_n(x,t)&=\frac{\bar{n}_n}{a_{33}'(\hat{\xi}_n)}\mathrm{e}^{-\mathrm{i}(\theta_1-\theta_2)(\xi_n)}. \end{aligned} \tag{80}$$

$$\begin{aligned} \check{F}_n(x,t)&=\frac{\check{f}_n b_{11}(z_n^*)}{a_{22}'(\hat{z}_n^*)}\mathrm{e}^{-\mathrm{i}(\theta_1+\theta_2)(z_n^*)},\\ \bar{F}_n(x,t)&=\frac{\bar{f}_n}{a_{22}'(\hat{z}_n)}\mathrm{e}^{\mathrm{i}(\theta_1+\theta_2)(z_n)},\\ N_n(x,t)&=\frac{n_n}{a_{11}'(\xi_n)}\mathrm{e}^{-\mathrm{i}(\theta_1-\theta_2)(\xi_n)},\\ \hat{N}_n(x,t)&=\frac{\hat{n}_n}{a_{22}'(\xi_n^*)}\mathrm{e}^{\mathrm{i}(\theta_1-\theta_2)(\xi_n^*)},\\ \check{N}_n(x,t)&=\frac{\check{n}_n}{a_{22}'(\hat{\xi}_n^*)}\mathrm{e}^{\mathrm{i}(\theta_1-\theta_2)(\xi_n^*)},\\ \bar{N}_n(x,t)&=\frac{\bar{n}_n}{a_{33}'(\hat{\xi}_n)}\mathrm{e}^{-\mathrm{i}(\theta_1-\theta_2)(\xi_n)}. \end{aligned} \tag{81}$$

4.2. Solution of the RHP

The solutions to the RHP defined by Eqs. (59)–(69) are expressed as

$$\begin{aligned} &M(x,t,z)\\ &=E_+(z)+\sum_{n=1}^{N}\left(\frac{M^{+}_{-1,v_n}}{z-v_n}+\frac{M^{-}_{-1,v_n^*}}{z-v_n^*}+\frac{M^{+}_{-1,\hat{v}_n^*}}{z-\hat{v}_n^*}+\frac{M^{-}_{-1,\hat{v}_n}}{z-\hat{v}_n}\right)\\ &\quad-\frac{1}{2\pi\mathrm{i}}\int_\Sigma\frac{M^{-}(\xi)}{\xi-z}\bar{L}(\xi)\mathrm{d}\xi, \end{aligned} \tag{82}$$

where $\{v_n\}_{n=1}^{N}$ are eigenvalues, $\bar{L}=\mathrm{e}^{\mathrm{i}\Theta}L\mathrm{e}^{-\mathrm{i}\Theta}$ and $M(x,t,z)=M^{\pm}(x,t,z)$. Futhermore, the eigenfunctions are derived under Eqs. (70)–(75):

$$\begin{aligned} \tau_2^{+}(x,t,z)=&\begin{pmatrix} 0 \\ \dfrac{1}{q_0}\boldsymbol{r}_+ \end{pmatrix}+\sum_{n=1}^{N_2}\left[\frac{\hat{F}_n}{z-z_n^*}-\frac{\mathrm{i}z_n^*}{q_0}\frac{\check{F}_n}{z-\hat{z}_n^*}\right]\tau_3^{-}(z_n^*)\\ &+\sum_{n=1}^{N_3}\left[\frac{\hat{N}_n}{z-\xi_n^*}-\frac{\mathrm{i}\xi_n^*}{q_0}\frac{\check{N}_n}{z-\hat{\xi}_n^*}\right]\tau_3^{-}(\xi_n^*)\\ &+\frac{1}{2\pi\mathrm{i}}\int_\Sigma\frac{(M^{-}\bar{L})_2(\xi)}{\xi-z}\mathrm{d}\xi, \end{aligned} \tag{83}$$

$$\begin{aligned} \tau_3^{-}(x,t,z)=&\begin{pmatrix} \dfrac{\mathrm{i}q_0}{z} \\ \dfrac{1}{q_0}\boldsymbol{q}_+ \end{pmatrix}+\sum_{n=1}^{N_1}\left[\frac{\hat{S}_n\tau_1^{-}(w_n^*)}{z-w_n^*}-\frac{\mathrm{i}w_n^*}{q_0}\frac{\bar{S}_n\tau_3^{+}(w_n^*)}{z-\hat{w}_n}\right]\\ &+\sum_{n=1}^{N_2}\left[\frac{F_n\tau_2^{+}(z_n)}{z-z_n}\right]+\sum_{n=1}^{N_3}\left[\frac{\bar{N}_n\tau_2^{+}(\xi_n)}{z-\hat{\xi}_n}\right]\\ &+\frac{1}{2\pi\mathrm{i}}\int_\Sigma\frac{(M^{-}\bar{L})_3(\xi)}{\xi-z}\mathrm{d}\xi, \end{aligned} \tag{84}$$

$$\begin{aligned} \tau_1^{-}(x,t,z)=&\begin{pmatrix} 1 \\ \dfrac{\mathrm{i}}{z}\boldsymbol{q}_+ \end{pmatrix}+\sum_{n=1}^{N_1}\left[\frac{S_n\tau_3^{+}(w_n)}{z-w_n}-\frac{\mathrm{i}w_n^*}{q_0}\frac{\check{S}_n\tau_1^{-}(w_n^*)}{z-\hat{w}_n^*}\right]\\ &+\sum_{n=1}^{N_2}\left[\frac{\bar{F}_n\tau_2^{+}(z_n)}{z-\bar{z}_n}\right]+\sum_{n=1}^{N_3}\left[\frac{N_n\tau_2^{+}(\xi_n)}{z-\xi_n}\right]\\ &+\frac{1}{2\pi\mathrm{i}}\int_\Sigma\frac{(M^{-}\bar{L})_1(\xi)}{\xi-z}\mathrm{d}\xi, \end{aligned} \tag{85}$$

$$\tau_3^+(x,t,z) = \begin{pmatrix} \frac{\mathrm{i}q_0}{z} \\ \frac{\mathrm{i}}{z}\boldsymbol{q}_+ \end{pmatrix} + \sum_{n=1}^{N_1}\left[\frac{\hat{S}_n\tau_1^-(w_n^*)}{z-w_n^*} - \frac{\mathrm{i}w_n^*}{q_0}\frac{\bar{S}_n\tau_3^+(w_n)}{z-\hat{w}_n}\right] + \sum_{n=1}^{N_2}\left[\frac{F_n\tau_2^+(z_n)}{z-z_n}\right] + \sum_{n=1}^{N_3}\left[\frac{\bar{N}_n\tau_2^+(\xi_n)}{z-\hat{\xi}_n}\right] + \frac{1}{2\pi\mathrm{i}}\int_\Sigma \frac{(M^-\bar{L})_3(\xi)}{\xi-z}\mathrm{d}\xi. \tag{86}$$

4.3. Formulae

The corresponding solutions q_k $(k=1,2)$ are

$$\begin{aligned} q_k(x,t) = {} & q_{+,k} - \mathrm{i}\sum_{j=1}^{N_1}\left[S_j m_{k+1,3}^+(w_j) + \check{S}_j m_{k+1,3}^+(\hat{w}_j^*)\right] \\ & - \mathrm{i}\sum_{j=1}^{N_2}\bar{F}_j m_{k+1,2}^+(\hat{z}_j) \\ & - \mathrm{i}\sum_{j=1}^{N_3} N_j m_{k+1,2}^+(\xi_j) \\ & - \frac{1}{2\pi}\sum_{j=1}^{4}\int_{\Sigma_j}\left(M^-\bar{L}_j\right)_{k+1,1}(\xi)\mathrm{d}\xi, \end{aligned} \tag{87}$$

and the trace formulas are given by

$$\begin{aligned} a_{11}(z) &= \mathrm{e}^{\varpi_1}\prod_{n=1}^{N_1}\frac{z-w_n}{z-w_n^*}\frac{z-\hat{w}_n^*}{z-\hat{w}_n}\prod_{n=1}^{N_2}\frac{z-\hat{z}_n}{z-\hat{z}_n^*}\prod_{n=1}^{N_3}\frac{z-\xi_n}{z-\xi_n^*}, \\ b_{22}(z) &= \mathrm{e}^{\varpi_2}\prod_{n=1}^{N_2}\frac{z-z_n}{z-z_n^*}\frac{z-\hat{z}_n^*}{z-\hat{z}_n}\prod_{n=1}^{N_3}\frac{z-\xi_n}{z-\xi_n^*}\frac{z-\hat{\xi}_n}{z-\hat{\xi}_n^*}, \end{aligned} \tag{88}$$

where

$$\varpi_1 = \frac{1}{2\pi\mathrm{i}}\int_\Sigma\frac{J(\xi)}{\xi-z}\mathrm{d}\xi,$$
$$\varpi_2 = -\mathrm{i}\Delta\theta - \frac{1}{2\pi\mathrm{i}}\int_R\frac{J_0(\xi)}{\xi-z}\mathrm{d}\xi,$$

and the jump conditions are defined as follows:

$$J_0(z) = \log\left[1+\eta(z)\rho_3(\hat{z})\rho_3^*(\hat{z}^*)+\eta(z)\rho_3(z)\rho_3^*(z^*)\right], \tag{89}$$

$$\Delta\theta = \frac{1}{2\pi}\int_\Sigma\frac{J(\xi)}{\xi}\mathrm{d}\xi - 4\sum_{n=1}^{N_1}\arg w_n + 2\sum_{n=1}^{N_2}\arg z_n - 2\sum_{n=1}^{N_3}\arg\xi_n. \tag{90}$$

When $J(z)=0$, the solution (87) can be rewritten as

$$\boldsymbol{q}(x,t) = \frac{1}{\det G}\begin{pmatrix}\det G_1^{\mathrm{aug}} \\ \det G_2^{\mathrm{aug}}\end{pmatrix}, \tag{91}$$

where $G = I - F$,

$$G_j^{\mathrm{aug}} = \begin{pmatrix} q_{+,k} & y^{\mathrm{T}} \\ b_k & G\end{pmatrix} \quad (j=1,2)$$

with

$$b_k = (b_{k,1},\ldots,b_{k,2N1+N2+N3})^{\mathrm{T}} \text{ and } y = (y_1,\ldots,y_{2N1+N2+N3})^{\mathrm{T}}.$$

Among which, $F=(F_{ij})$ with F_{ij} being easily obtained.

The coefficients $G_n^{(k)}$ $(k=1,\ldots,10,\ n=1,\ldots,\max\{N_1,N_2,N_3\})$ are

$$\begin{aligned} G_n^{(1)}(x,t,z) &= \frac{\hat{F}_n(x,t)}{z-z_n^*} - \frac{\mathrm{i}z_n^*}{q_0}\frac{\check{F}_n(x,t)}{z-\hat{z}_n^*}, \\ G_n^{(2)}(x,t,z) &= \frac{\hat{N}_n(x,t)}{z-\xi_n^*} - \frac{\mathrm{i}\xi_n^*}{q_0}\frac{\check{N}_n(x,t)}{z-\hat{\xi}_n^*}, \\ G_n^{(3)}(x,t,z) &= \frac{\hat{S}_n(x,t)}{z-w_n^*}, \\ G_n^{(4)}(x,t,z) &= -\frac{\mathrm{i}w_n}{q_0}\frac{\bar{S}_n(x,t)}{z-\hat{w}_n}, \\ G_n^{(5)}(x,t,z) &= \frac{F_n(x,t)}{z-z_n}, \quad G_n^{(6)}(x,t,z) = \frac{\bar{N}_n(x,t)}{z-\hat{\xi}_n}, \\ G_n^{(7)}(x,t,z) &= \frac{S_n(x,t)}{z-w_n}, \quad G_n^{(8)}(x,t,z) = -\frac{w_n^*}{q_0}\frac{\check{S}_n(x,t)}{z-\hat{w}_n^*}, \\ G_n^{(9)}(x,t,z) &= \frac{\bar{F}_n(x,t)}{z-\hat{z}_n}, \quad G_n^{(10)}(x,t,z) = \frac{N_n(x,t)}{z-\xi_n}, \\ & n=1,\ldots,\max\{N_1,N_2,N_3\}. \end{aligned} \tag{92}$$

5. Solutions for Eq. (2)

By selecting $N_2=1$, $N_1=0$, and $N_3=0$, one-soliton solutions have the forms as

$$\boldsymbol{q}(x,t) = \frac{1}{\det G}\begin{pmatrix}\det G_1^{\mathrm{aug}} \\ \det G_2^{\mathrm{aug}}\end{pmatrix}, \tag{93}$$

where

$$\det G_k^{\mathrm{aug}} = \begin{pmatrix} q_{+,k} & y^{\mathrm{T}} \\ b_k & G\end{pmatrix},$$
$$G = 1 - F_{11},\ \ y^{\mathrm{T}} = y_1,\ \ b_k = b_{k1}\ (k=1,2).$$

Setting

$$q = \begin{pmatrix}1\\0\end{pmatrix},\quad f_1 = \mathrm{e}^{\zeta+\mathrm{i}\xi},\quad z_1 = \beta\,\mathrm{e}^{\mathrm{i}\alpha}, \tag{94}$$

we can simplify to the following form:

$$q_1 = \frac{V_1+\cosh(\Xi_1+2\zeta)+\sinh(\Xi_1+2\zeta)}{V_1+\cosh(\Xi_1+2\zeta+2\mathrm{i}\alpha)+\sinh(\Xi_1+2\zeta+2\mathrm{i}\alpha)}, \tag{95}$$

$$q_2 = V_5\frac{\cosh(\Xi_2+\zeta+\mathrm{i}\xi+2\mathrm{i}\alpha)+\sinh(\Xi_2+\zeta+\mathrm{i}\xi+2\mathrm{i}\alpha)}{V_4+\cosh(\Xi_1+2\zeta+2\mathrm{i}\alpha)+\sinh(\Xi_1+2\zeta+2\mathrm{i}\alpha)}, \tag{96}$$

where

$$\begin{aligned} \Xi_1 &= -(\Delta_1+\Delta_1^*)x + (\Delta_2+\Delta_2^*)\int\sigma(t)\mathrm{d}t \\ &\quad + (4\Delta_2+4\Delta_2^*-\Delta_4-\Delta_4^*)\int\gamma_1(t)\mathrm{d}t, \\ \Xi_2 &= -\Delta_1 x + \Delta_2\int\sigma(t)\mathrm{d}t + (4\Delta_2-\Delta_4)\int\gamma_1(t)\mathrm{d}t, \\ V_1 &= \frac{\varepsilon_{0,2}+\varepsilon_{2,0}+\varepsilon_{4,2}+\varepsilon_{2,4}}{\varepsilon_{0,2}+\varepsilon_{0,4}}, \end{aligned}$$

$$V_4 = \frac{\varepsilon_{0,2}+\varepsilon_{2,0}+\varepsilon_{2,2}+\varepsilon_{2,4}}{\varepsilon_{0,2}+\varepsilon_{0,4}},$$
$$V_5 = \frac{\varepsilon_{2,4}+\varepsilon_{4,0}+\varepsilon_{4,2}-\varepsilon_{0,2}-\varepsilon_{2,0}-\varepsilon_{0,4}}{\varepsilon_{0,2}+\varepsilon_{0,4}},$$

with $\Delta_j = (\mathrm{i}\,\mathrm{e}^{-j\mathrm{i}\alpha})/\beta^j$ and $\varepsilon_{k,l} = \mathrm{e}^{k\mathrm{i}\alpha}\beta^l$.

When $\alpha = \pi/2$, a distinctive pair of bright–dark solitons is discernible, as depicted in Fig. 1. In this scenario, they remain immobile, and irrespective of modifications on $\sigma(t)$ and $\gamma_1(t)$, they persist in their stationary state. Furthermore, we consider the velocities of the solitons q_1 and q_2 to be denoted by

$$(\Delta_2+\Delta_2^*)\sigma(t)+(4\Delta_2+4\Delta_2^*-\Delta_4-\Delta_4^*)\gamma_1(t)/(\Delta_1+\Delta_1^*),$$
$$\Delta_2\sigma(t)+(4\Delta_2-\Delta_4)\gamma_1(t)/\Delta_1,$$

respectively. It can be inferred that when $\alpha = \pi/2$, the velocities are constants. Consequently, subsequent discussions will be conducted on the premise that $\alpha \neq \pi/2$.

When $\alpha = \pi/3$, figure 2 illustrates a moving pair of the bright–dark solitons. We will select a series of foundational functions to illustrate the variations in the soliton states.

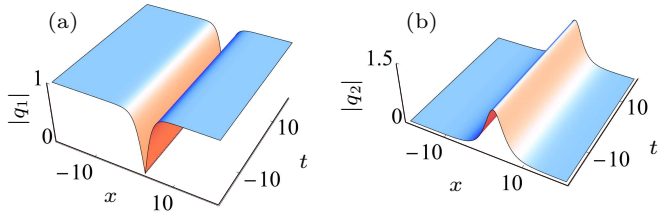


Fig. 1. Bright–dark solitons for solutions (95)–(96) with $\alpha = \pi/2$, $\beta = 2$, $\zeta = 1$, $\xi = 1$, $\sigma(t) = 1$, and $\gamma_1(t) = 1$.

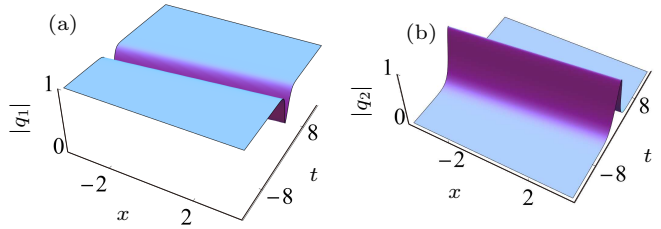


Fig. 2. Bright–dark solitons for solutions (95)–(96) with $\alpha = \pi/3$, $\beta = 2$, $\zeta = 1$, $\xi = 1$, $\sigma(t) = 1$, and $\gamma_1(t) = 1$.

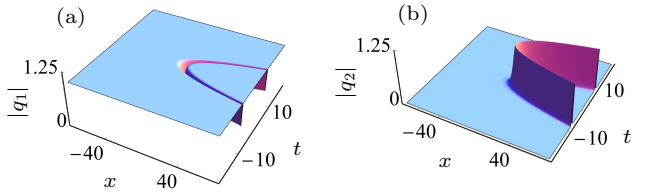


Fig. 3. Bright–dark solitons for solutions (95)–(96) with $\alpha = \pi/3$, $\beta = 2$, $\zeta = 1$, $\xi = 1$, $\sigma(t) = t$, and $\gamma_1(t) = t$.

Considering the previously derived expressions, the influence of $\sigma(t)$ and $\gamma_1(t)$ on soliton motion is analogous. Here, we focus solely on $\sigma(t)$ for a more concise discussion. When $\sigma(t)$ is selected as a linear function, as shown in Fig. 3, the direction of the soliton velocity in Fig. 3 becomes opposite at the origin of the coordinate axis. Moreover, as it approaches the origin, the soliton velocity decreases, conforming to a parabolic variation pattern.

If we choose $\sigma(t)$ as a quadratic function, as depicted in Fig. 4, the soliton exhibits distinctive behavior compared to the previous scenario. Although the speed varies as it approaches zero, the direction of the velocity remains unchanged throughout, aligning with the characteristic motion pattern of a regressive parabola.

When $\sigma(t)$ is chosen as a Gaussian function, as illustrated in Fig. 5, it portrays a soliton with exponentially increasing speed, and it exhibits a brief movement when approaching zero on the negative half-axis, but the velocity experiences explosive growth from zero onwards. Importantly, the direction of the velocity remains unchanged from start to finish, and aligning with the characteristic motion pattern of a Gaussian function.

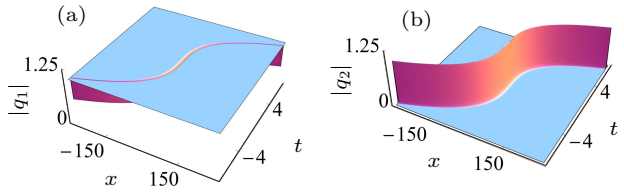


Fig. 4. Bright–dark solitons for solutions (95)–(96) with parameters $\alpha = \pi/3$, $\beta = 2$, $\zeta = 1$, $\xi = 1$, $\sigma(t) = t^2$, and $\gamma_1(t) = t^2$.

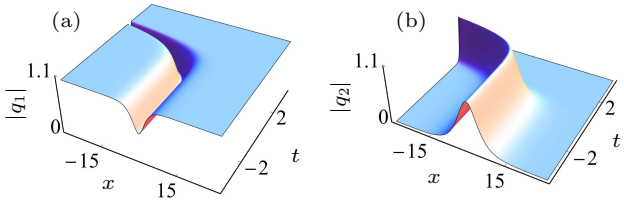


Fig. 5. Bright–dark solitons for solutions (95)–(96) with parameters $\alpha = \pi/3$, $\beta = 2$, $\zeta = 1$, $\xi = 1$, $\sigma(t) = -\mathrm{e}^t$, and $\gamma_1(t) = -\mathrm{e}^t$.

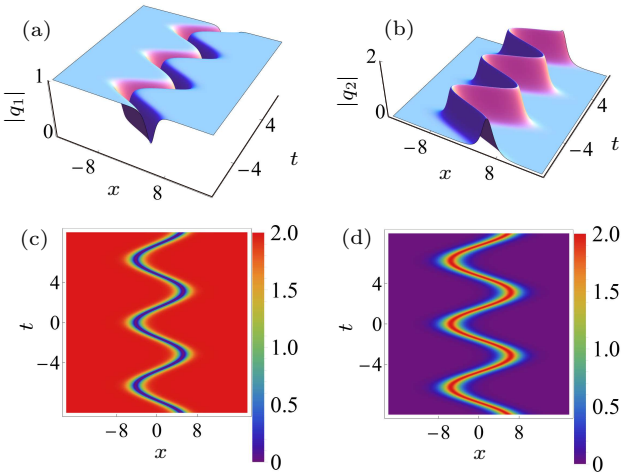


Fig. 6. Bright–dark solitons for solutions (95)–(96) with $\alpha = \pi/3$, $\beta = 2$, $\zeta = 1$, $\xi = 1$, $\sigma(t) = \sin(t)$, and $\gamma_1(t) = \sin(t)$.

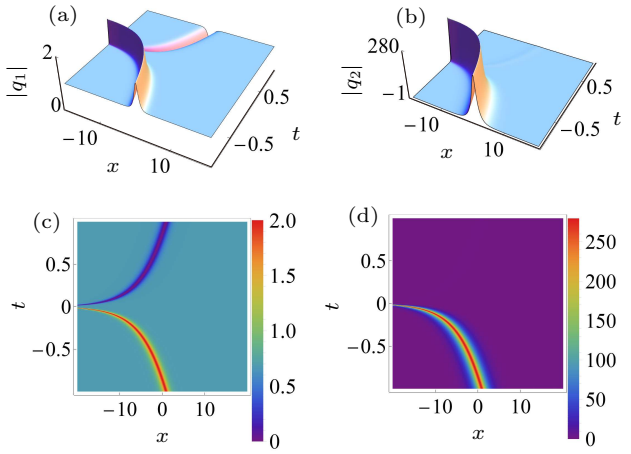


Fig. 7. Bright–dark solitons for solutions (95)–(96) with parameters $\alpha = \pi/3$, $\beta = 2$, $\zeta = 1$, $\xi = 1$, $\sigma(t) = 1/t$, and $\gamma_1(t) = 1$.

Previously, when altering $\sigma(t)$, results similar to those under zero boundary conditions were obtained. However, when $\sigma(t)$ is selected as a trigonometric function, as depicted in Fig. 6, a pair of solitons with a periodically changing velocity emerges. Referring to the expressions for the velocities of solitons q_1 and q_2, it can be observed that as the velocity approaches the peak of the trigonometric function, the speed towards infinity. Additionally, the amplitude undergoes a variation as the speed approaches infinity, and the soliton changes its velocity direction when at the trough of the trigonometric function.

Finally, in the case $\sigma(t)$ being a negative power function, a pair of solitons that do not hold under zero boundary conditions are observed. Interestingly, when the soliton approaches zero, both the speed and amplitude undergo changes tending towards infinity. The originally dark soliton q_1 forms a convexity resembling a bright soliton, while the originally bright soliton q_2 forms a concavity resembling a dark soliton.

Choosing $N_1 = 1, N_2 = 0$, and $N_3 = 0$, one-soliton solutions have the forms

$$\boldsymbol{q}(x,t) = \frac{1}{\det G}\begin{pmatrix} \det G_1^{\text{aug}} \\ \det G_2^{\text{aug}} \end{pmatrix}, \tag{97}$$

where

$$\det G_k^{\text{aug}} = \begin{pmatrix} q_{+,k} & y^{\mathrm{T}} \\ b_k & G \end{pmatrix}, \quad G = 1 - F_{11},$$
$$y^{\mathrm{T}} = y_1, \quad b_k = b_{k1} \quad (k = 1,2). \tag{98}$$

Assuming that $q = \begin{pmatrix} 1 \\ 0 \end{pmatrix}$, $f_1 = \mathrm{e}^{\zeta + \mathrm{i}\xi}$, and $z_1 = \beta\,\mathrm{e}^{\mathrm{i}\alpha}$, then we have

$$q_1 = \frac{V_6 + (\mathrm{e}^{6\mathrm{i}\alpha+\zeta} + \mathrm{e}^{8\mathrm{i}\alpha+\zeta})\Upsilon(A_1^*) + \beta^4(\mathrm{e}^{2\mathrm{i}\alpha+\zeta+2\mathrm{i}\xi} + \mathrm{e}^{4\mathrm{i}\alpha+\zeta+2\mathrm{i}\xi})\Upsilon(A_1) + \mathrm{e}^{3\mathrm{i}\alpha+\mathrm{i}\xi}(\beta+\beta^3)\Upsilon(A_1+A_1^*)}{V_7 + \beta^2(\mathrm{e}^{4\mathrm{i}\alpha+\zeta} + \mathrm{e}^{6\mathrm{i}\alpha+\zeta})\Upsilon(A_1^*) + \beta^2(\mathrm{e}^{\zeta+2\mathrm{i}\xi} + \mathrm{e}^{2\mathrm{i}\alpha+\zeta+2\mathrm{i}\xi})\Upsilon(A_1) + \mathrm{e}^{3\mathrm{i}\alpha+\mathrm{i}\xi}(\beta+\beta^3)\Upsilon(A_1+A_1^*)}, \tag{99}$$

$$q_2 = 0, \tag{100}$$

where $\Upsilon(x) = \cosh(x) + \sinh(x)$, $A_1 = -\Delta k(-1)x + \Delta k(1)x + \mathrm{i}\Delta k(-4)\int\gamma_1(t)\,\mathrm{d}t + 4\mathrm{i}\Delta k(-2)\int\gamma_1(t)\,\mathrm{d}t - 4\mathrm{i}\Delta k(2)\int\gamma_1(t)\,\mathrm{d}t - \mathrm{i}\Delta k(4)\int\gamma_1(t)\,\mathrm{d}t + \mathrm{i}\Delta k(-2)\int\sigma(t)\,\mathrm{d}t - \mathrm{i}\Delta k(2)\int\sigma(t)\,\mathrm{d}t$ and $\Delta k(x) = \mathrm{e}^{x\mathrm{i}\alpha}\beta^x$.

Since q_2 represents the plane wave, for the sake of simplicity in discussion, only q_1 will be addressed in the following. When the coefficients $\sigma(t)$ and $\gamma_1(t)$ are constants, choosing $\alpha = 0$ yields a special case of a breathing solitary wave with zero velocity, as depicted in Fig. 8(a), and as time progresses, the amplitude remains unchanged. On the other hand, it produces a breathing solitary wave with velocity with choosing $\alpha = \pi/3$, as shown in Fig. 8(b), which changes displacement at a fixed amplitude and velocity. Figures 8(c) and 8(d) provide a clearer depiction of the amplitude variation of the breathers during propagation. It can be observed that when the velocity is zero, as shown in Fig. 8(c), the breathers continuously appears and disappears with time, perpetually cycling through this process. When the velocity is nonzero, as depicted in Fig. 8(d), the breathers undergoes a similar cycle of emergence and disappearance, but displacement occurring.

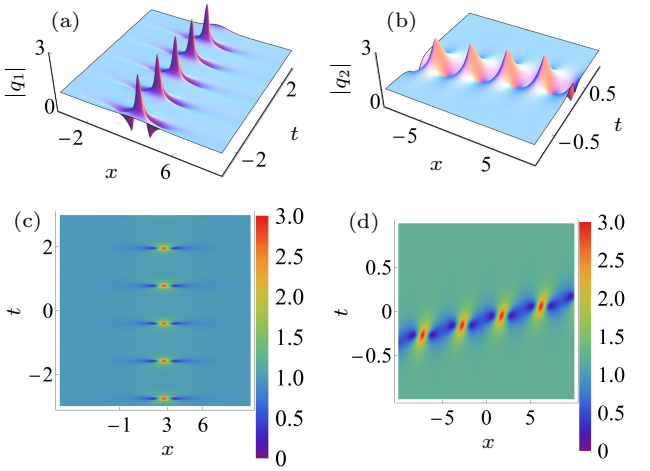


Fig. 8. Breathers for solution (99) with parameters (a) $\alpha = 0$, $\beta = 2$, $\zeta = 1$, $\xi = 1$, $\sigma(t) = 1$, and $\gamma_1(t) = 1$; (b) $\alpha = \pi/3$, $\beta = 2$, $\zeta = 1$, $\xi = 1$, $\sigma(t) = 1$, and $\gamma_1(t) = 1$.

If the coefficients $\sigma(t)$ and $\gamma_1(t)$ are quadratic functions, the discussion is similarly divided into cases where the velocity is zero and nonzero. In the case of zero velocity, as shown in Fig. 9(a), it can be observed that the breathing solitary wave exists in the form of a variable period, with the period increasing as it approaches zero. When the velocity is nonzero, as de-

picted in Fig. 9(b), the solitary wave exhibits uniform periodic motion, while maintaining constant amplitude in both scenarios. Figures 9(c) and 9(d) provide a more detailed illustration of the amplitude variation of the variable-period breathers during propagation.

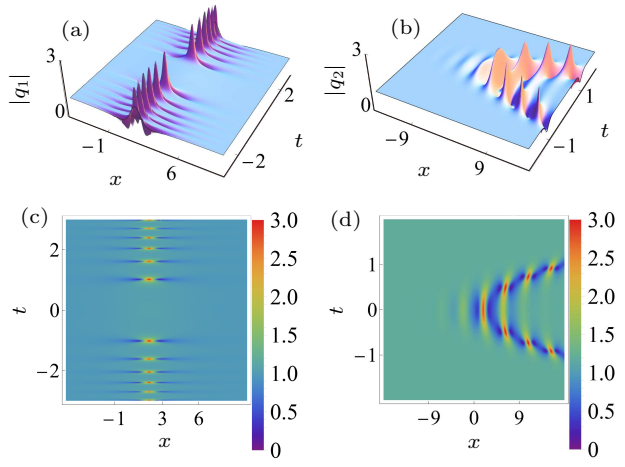


Fig. 9. Breather for solution (99) with parameters: (a) $\alpha=0$, $\beta=2$, $\zeta=1$, $\xi=1$, $\sigma(t)=t$, and $\gamma_1(t)=t$; (b) $\alpha=\pi/3$, $\beta=2$, $\zeta=1$, $\xi=1$, $\sigma(t)=t$, and $\gamma_1(t)=t$.

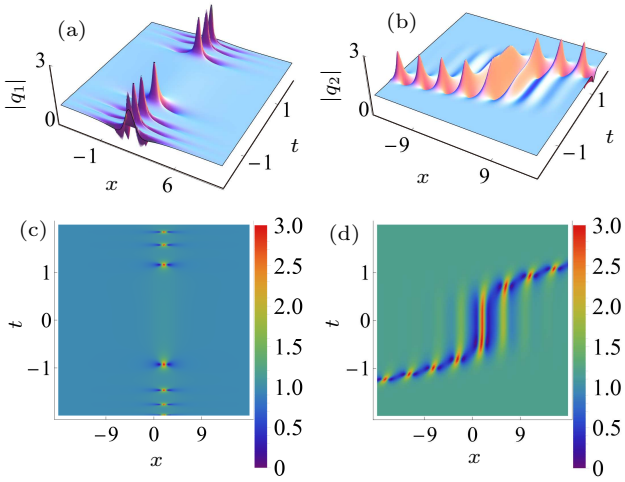


Fig. 10. Breather for solution (99) with parameters: (a) $\alpha=0$, $\beta=2$, $\zeta=1$, $\xi=1$, $\sigma(t)=t^2$, and $\gamma_1(t)=t^2$; (b) $\alpha=\pi/3$, $\beta=2$, $\zeta=1$, $\xi=1$, $\sigma(t)=t^2$, and $\gamma_1(t)=t^2$.

If the coefficients $\sigma(t)$ and $\gamma_1(t)$ are modified to cubic functions, the variation in period when the velocity is zero becomes more pronounced. Conversely, when the velocity is nonzero, the direction of the breathing solitary wave's velocity remains unchanged, but its velocity value is dependent on the cubic function.

When the coefficients $\sigma(t)$ and $\gamma_1(t)$ are modified to Gaussian functions, the motion of the breathing solitary wave conforms to the variation pattern of the Gaussian function. Prior to zero crossing, the velocity undergoes minimal changes, while after crossing zero, the velocity experiences drastic variations in magnitude.

If the coefficients $\sigma(t)$ and $\gamma_1(t)$ are set to trigonometric functions, compared to the scenario where the amplitude remains constant during the motion of the breather, in this case, when the velocity value is zero, the amplitude of the breather changes with the period. Similarly, when the velocity value is nonzero, the amplitude also varies with the period, and the motion direction exhibits periodic changes in accordance with the trigonometric function.

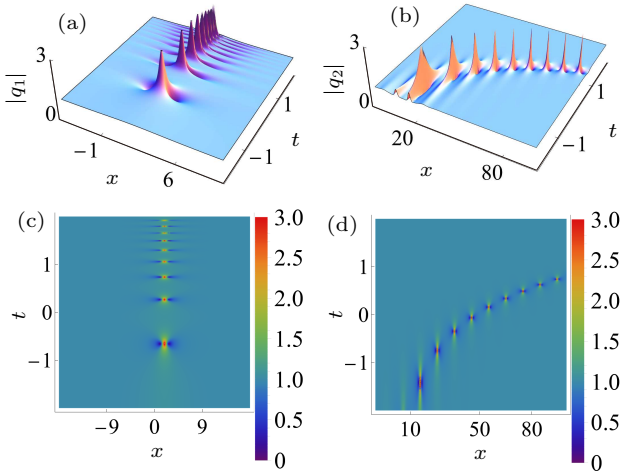


Fig. 11. Breather for solution (99) with parameters (a) $\alpha=0$, $\beta=2$, $\zeta=1$, $\xi=1$, $\sigma(t)=\mathrm{e}^t$, and $\gamma_1(t)=\mathrm{e}^t$; (b) $\alpha=\pi/3$, $\beta=2$, $\zeta=1$, $\xi=1$, $\sigma(t)=\mathrm{e}^t$, and $\gamma_1(t)=\mathrm{e}^t$.

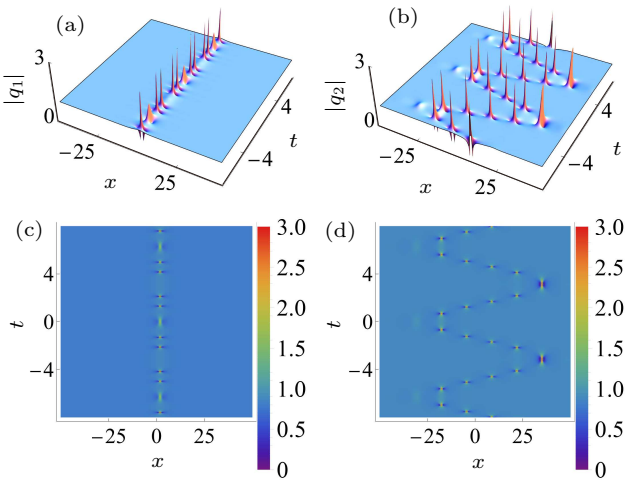


Fig. 12. Breather for solution (99) with parameters (a) $\alpha=0$, $\beta=2$, $\zeta=1$, $\xi=1$, $\sigma(t)=\sin(t)$, and $\gamma_1(t)=\sin(t)$; (b) $\alpha=\pi/3$, $\beta=2$, $\zeta=1$, $\xi=1$, $\sigma(t)=\sin(t)$, and $\gamma_1(t)=\sin(t)$.

Choosing $N_3=2$, $N_1=0$ and $N_2=0$, two-soliton solutions are

$$\boldsymbol{q}(x,t)=\frac{1}{\det G}\begin{pmatrix}\det G_1^{\mathrm{aug}}\\ \det G_2^{\mathrm{aug}}\end{pmatrix}, \tag{101}$$

where

$$\det G_k^{\mathrm{aug}}=\begin{pmatrix}q_{+,k} & y^{\mathrm{T}}\\ b_k & G\end{pmatrix},\quad G=1-F_{11},$$
$$y^{\mathrm{T}}=\begin{pmatrix}y_1 & y_2\end{pmatrix},\quad b_k=\begin{pmatrix}b_{k1} & b_{k2}\end{pmatrix}^{\mathrm{T}}\quad (k=1,2). \tag{102}$$

For simplicity, we choose $q = \begin{pmatrix} 1 \\ 0 \end{pmatrix}$, $f_1 = \mathrm{e}^{\zeta_1 + \mathrm{i}\xi_1}$, $z_1 = \beta_1 \mathrm{e}^{\mathrm{i}\alpha_1}$, $f_2 = \mathrm{e}^{\zeta_2 + \mathrm{i}\xi_2}$, and $z_2 = \beta_2 \mathrm{e}^{\mathrm{i}\alpha_2}$.

When discussing simple pole two solitons, we only consider the case of $N_3 = 2$. In this scenario, interesting nonlinear phenomena arise. When the coefficients $\sigma(t)$ and $\gamma_1(t)$ are constants, we observe two distinct scenarios in Figs. 13 and 14. Figures 13 demonstrates elastic collisions between solitons, where the amplitude remains unchanged before and after collision, producing a high wave in the center. In contrast, figure 14 exhibits different behaviors: in Fig. 14(a), the solitons transform into breathing solitary waves after collision, exhibiting periodic propagation, while in Fig. 14(b), the solitons vanish after mutually canceling each other out post-collision.

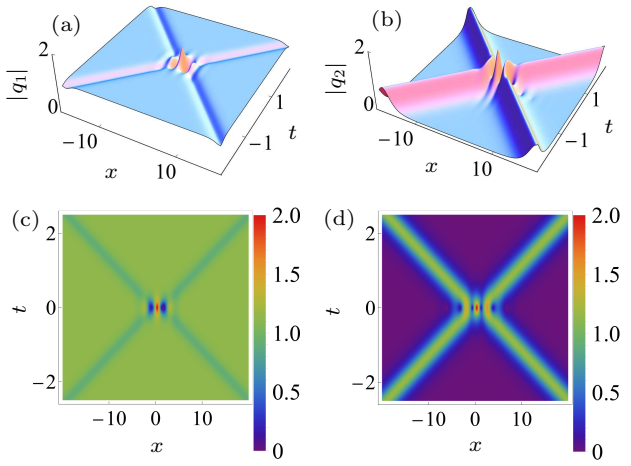


Fig. 13. Collisions between the vector two solitons via solutions (101)–(102), (a)–(d) $\alpha_1 = \pi/3$, $\beta_1 = 1$, $\zeta_1 = 1$, $\xi_1 = 1$, $\alpha_2 = -\pi/3$, $\beta_2 = 1$, $\zeta_2 = 1$, $\xi_2 = 1$, $\sigma(t) = 1$, and $\gamma_1(t) = 1$.

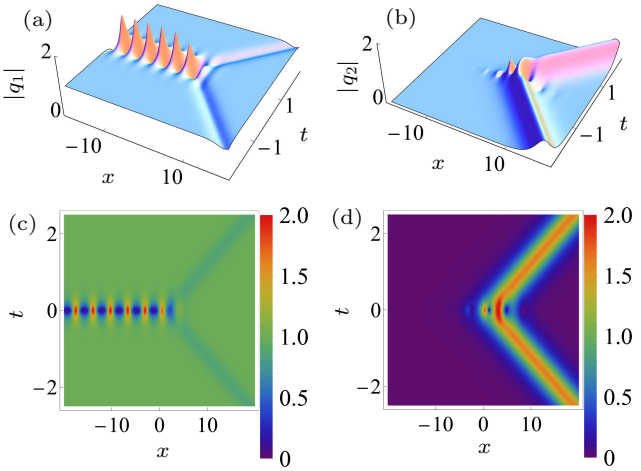


Fig. 14. Collisions between the vector two solitons via solutions (101)–(102), (a)–(d) $\alpha_1 = \pi/3$, $\beta_1 = 5/4$, $\zeta_1 = 1$, $\xi_1 = 1$, $\alpha_2 = -\pi/3$, $\beta_2 = 5/4$, $\zeta_2 = 1$, $\xi_2 = 1$, $\sigma(t) = 1$, and $\gamma_1(t) = 1$.

When the coefficients $\sigma(t)$ and $\gamma_1(t)$ are quadratic or cubic functions, similar phenomena occur. Here, we only demonstrate the case of quadratic functions. When other coefficients are varied, two scenarios are depicted in Figs. 15 and 16. Figure 15 differs from Fig. 14 in that the resulting breathing solitary wave has a wider width, and the velocity variation before interaction follows a parabolic pattern. On the other hand, figure 16 diverges from Fig. 13 in that the velocity variation before collision also follows a parabolic pattern, and after collision, the solitons do not immediately separate but instead maintaining a high wave form for a period of time, during which the solitons remain stationary.

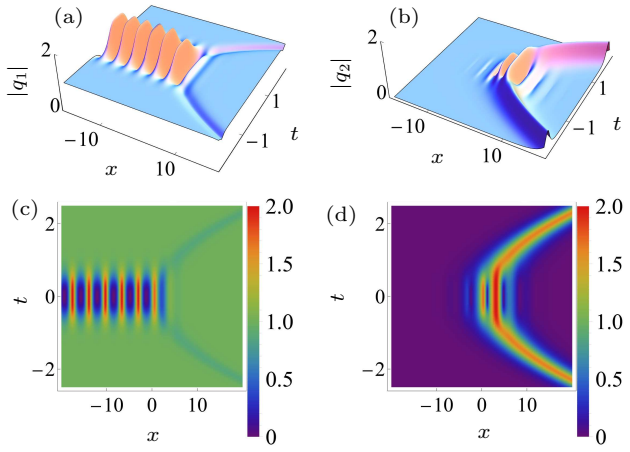


Fig. 15. Parameters are the same as Fig. 14 except that $\sigma(t) = t$ and $\gamma_1(t) = t$.

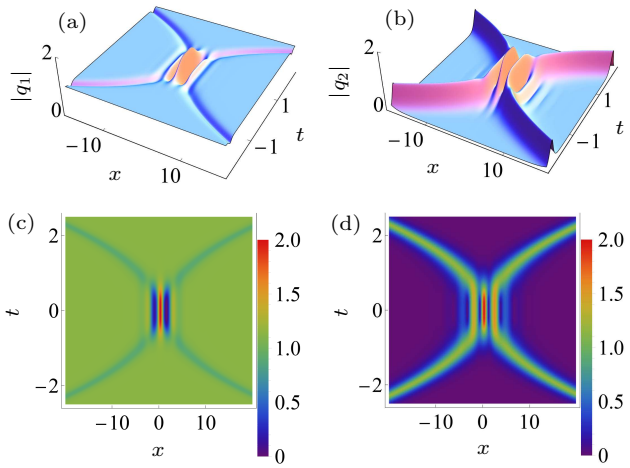


Fig. 16. Parameters are the same as Figs. 13 except that $\sigma(t) = t$ and $\gamma_1(t) = t$.

When setting $\sigma(t)$ and $\gamma_1(t)$ as trigonometric functions, as shown in Fig. 17, two types of nonlinear phenomena emerge. First type involves solitons forming breather-like solitons after each interaction, followed by separating from each other again. The other type involves the formation of two-peak solitons after interaction, followed by their separation over time. Both phenomena exhibit periodic behavior with respect to the trigonometric function. Furthermore, the soliton dynamics depicted in Fig. 17 exhibits a considerable correlation with those in Fig. 16. In q_1, solitons form high-amplitude breather-like solitons after interaction, while in q_2, solitons cancel each other out, resulting in reduced amplitude until the soliton dis-

appears. However, in Figs. 17(b) and 17(d), the velocity direction undergoes continuous changes in a trigonometric manner. Therefore, solitons do not disappear after interaction but transforming into low-amplitude two-peak solitons. Subsequently, they separate after the velocity direction changes, initiating the next cycle of interaction.

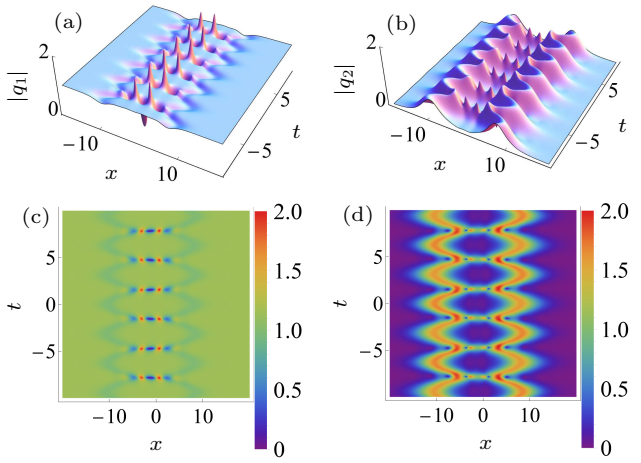


Fig. 17. Parameters are the same as Fig. 13 except that $\sigma(t) = \sin(t)$ and $\gamma_1(t) = \sin(t)$.

When we modify some coefficients while keeping the variable coefficients unchanged, which depicted in Fig. 18. It resembles the behavior observed in Figs. 13(a) and 13(b), recurring periodically in Fig. 18. After interaction, solitons generate a high wave, which then continue to propagate in the same direction. Furthermore, the subsequent motion of individual solitons follows a trigonometric pattern.

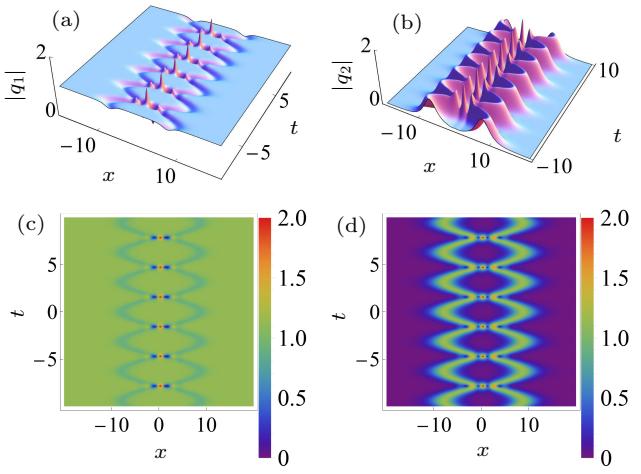


Fig. 18. Parameters are the same as Figs. 14 except that $\sigma(t) = \sin(t)$ and $\gamma_1(t) = \sin(t)$.

The majority of the nonlinear phenomena described above arise from interactions between solitons moving in opposite initial directions. If we alter the initial motion directions of the solitons to make the angle between them smaller than a right angle, different nonlinear phenomena occur, as illustrated in Fig. 19. In this case, the coefficients $\sigma(t)$ and $\gamma_1(t)$ are both constants. It can be observed that the two solitons experience a repulsion just before they are about to interact. As a result, they do not interact with each other and no high wave is generated. However, after the repulsion, the solitons exchange their amplitudes, and this phenomenon occurs in both bright and dark solitons.

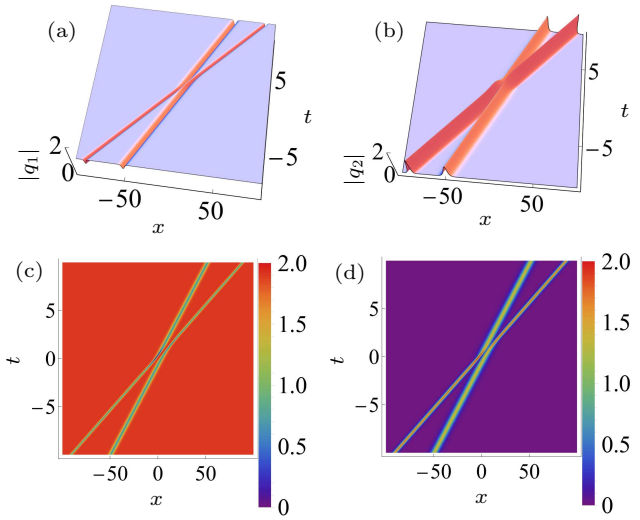


Fig. 19. Parameters are the same as Fig. 13 except that $\alpha_1 = \pi/4$, $\beta_1 = 5/4$, $\zeta_1 = 0$, $\xi_1 = 0$, $\alpha_2 = 3\pi/4$, $\beta_2 = 4/5$, $\zeta_2 = 0$, and $\xi_2 = 0$.

Next, we modify the coefficients $\sigma(t)$ and $\gamma_1(t)$ to be basic functions, as depicted in Fig. 20, where the coefficients are quadratic functions. In this case, it can be observed that unlike Fig. 19, the two solitons do not interact with each other just before they interact, as the soliton changing faster in speed in the inner loop does not interact with the other soliton, nor does it experience repulsion. However, as they approach the zero point, there is a certain degree of energy exchange.

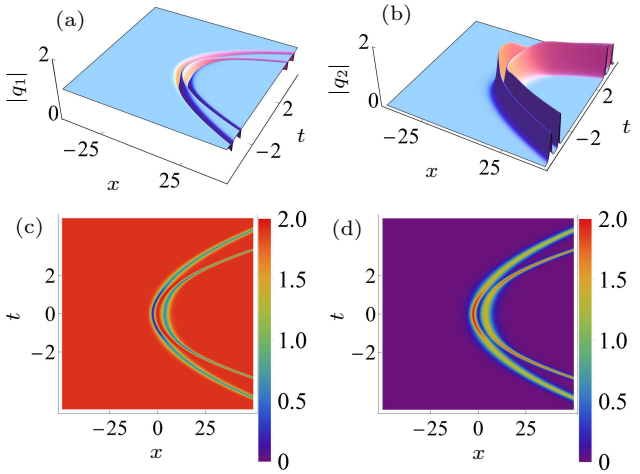


Fig. 20. Parameters are the same as Fig. 19 except that $\sigma(t) = t$ and $\gamma_1(t) = t$.

When employing cubic functions, as depicted in Fig. 21, the soliton dynamics are similar to those in Fig. 20, as there is no interaction between the solitons and no repulsion phenomenon occurs. This is because as they approach the zero

point, the soliton that was originally faster decelerates more rapidly, while the slower soliton decelerates at a slower rate. Conversely, as they move away from the original point, the velocity patterns of the two solitons are exchanged. Additionally, within the vicinity of the zero point, there is also an exchange of energy between the two solitons.

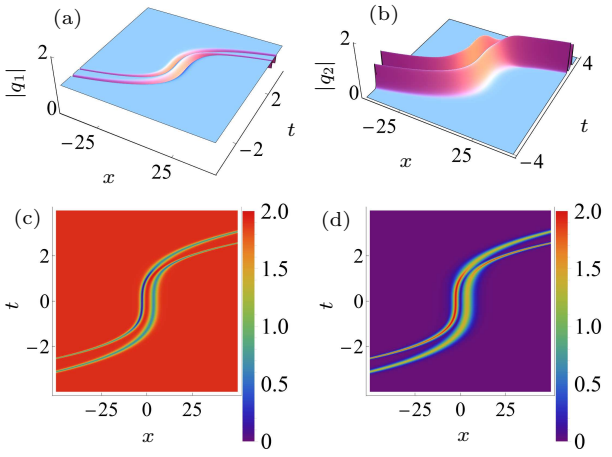


Fig. 21. Parameters are the same as Fig. 19 except that $\sigma(t) = t^2$ and $\gamma_1(t) = t^2$.

If $\sigma(t)$ and $\gamma_1(t)$ are Gaussian functions, the soliton dynamics are illustrated in Fig. 22. It can be observed that before approaching the zero point, the two solitons remain stationary in the form of parallel solitons with different amplitudes. However, after moving away from the zero point, energy exchange occurs between the two solitons, and their velocities change according to the Gaussian function. Nonetheless, there is still no interaction or repulsion between the two solitons.

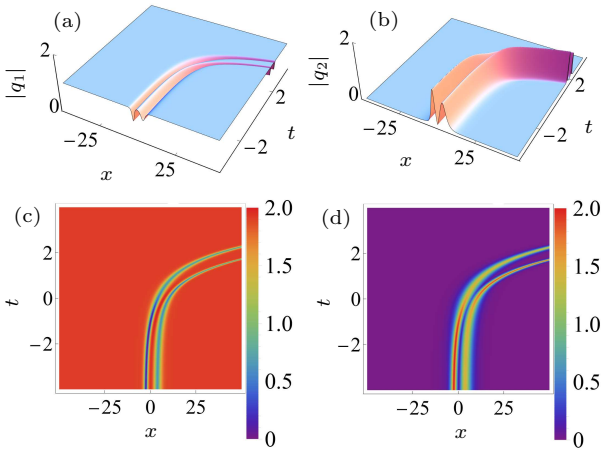


Fig. 22. Parameters are the same as Fig. 19 except that $\sigma(t) = \mathrm{e}^t$ and $\gamma_1(t) = \mathrm{e}^t$.

If $\sigma(t)$ and $\gamma_1(t)$ are trigonometric functions, the soliton dynamics are revealed as depicted in Fig. 23. It can be observed that soliton motion resembles parallel solitons but undergoes periodic oscillations according to the trigonometric function. Energy exchange occurs when the trigonometric function approaches its minimum, with narrower solitons experiencing a decrease in energy and amplitude while wider solitons experience an increase in energy with unchanged amplitude and increased width. Conversely, energy remains unchanged when the trigonometric function reaches its peak. Furthermore, upon leaving the minimum, energy exchange occurs again, following the opposite pattern observed when approaching the minimum, and this exchange pattern follows the behavior of the trigonometric function.

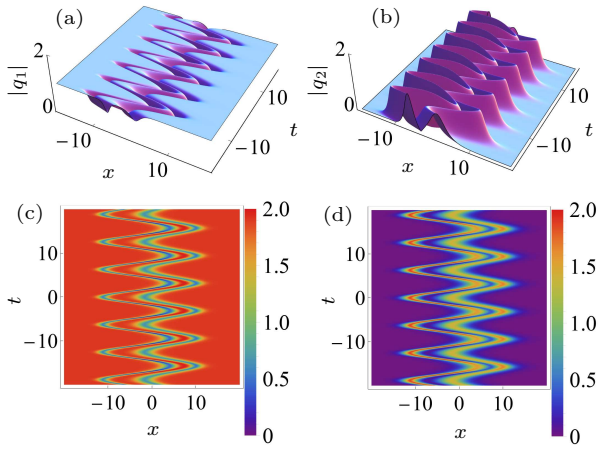


Fig. 23. Parameters are the same as Fig. 19 except that $\sigma(t) = \sin(t)$ and $\gamma_1(t) = \sin(t)$.

If we maintain the direction of soliton motion and increase the strength of soliton interactions, interesting phenomena occur as shown in Fig. 24. At this point, q_1 and q_2 no longer correspond to a simple relationship between bright and dark solitons. After the interaction in q_1, there is no generation of a high wave, but rather a depression downward and a decrease in amplitude. This suggests that higher-energy solitons do not necessarily produce higher waves after interaction. Instead, elastic collisions between solitons with energy above a certain threshold can lead to depressions. In q_2, two high-energy solitons experience a rebound just before their interaction, with the solitons moving in opposite directions. At this moment, each soliton produces a high wave without energy exchange occurring.

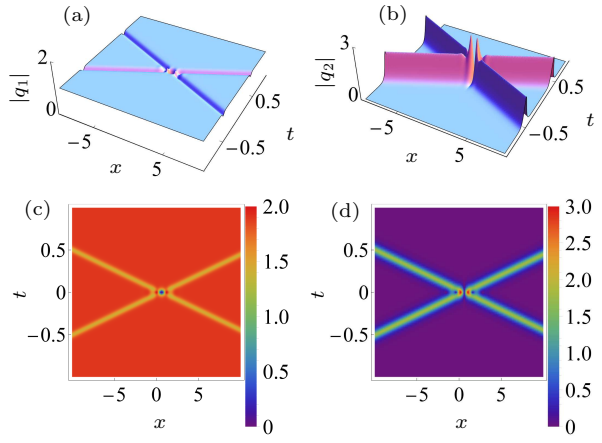


Fig. 24. Parameters are the same as Fig. 13 except that $\beta_1 = 1.1$, $\beta_2 = 3$.

Next, we modify the functions $\sigma(t)$ and $\gamma_1(t)$ to observe the motion pattern of solitons. The results obtained with quadratic and cubic functions are similar, so we only discuss the case of quadratic functions here, as shown in Fig. 25. In this case, we observed that the motion patterns of the two solitons follow quadratic functions. In Fig. 25(a), the depression generated by the interaction between solitons persists for a period, while in Fig. 25(b), the solitons maintain a high wave pattern for some time before rebounding.

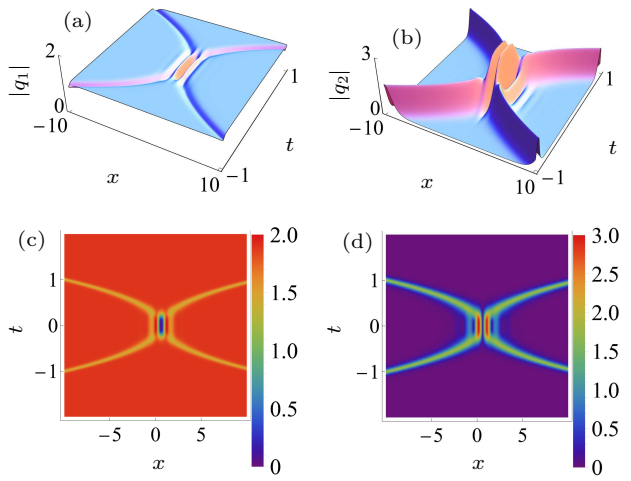


Fig. 25. Parameters are the same as Fig. 24 except that $\sigma(t) = t$ and $\gamma_1(t) = t$.

Finally, when the coefficients are trigonometric functions, we revealed the phenomenon shown in Fig. 26. It resembles a continuous recurrence of the pattern observed in Fig. 24. In Fig. 26(a), a depression forms after each interaction, and then the solitons separate to continue the next interaction cycle. Conversely, in Fig. 26(b), the solitons immediately rebound when they are about to interact, and high waves are generated at their proximity.

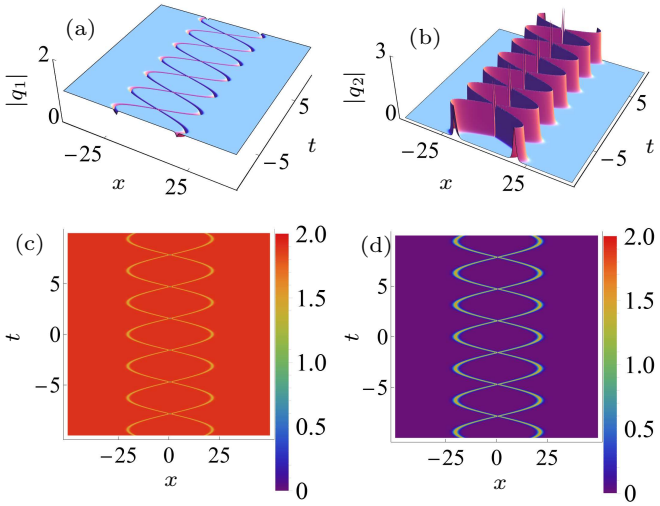


Fig. 26. Parameters are the same as Fig. 24 except that $\sigma(t) = \sin(t)$ and $\gamma_1(t) = \sin(t)$.

6. Conclusions

In this study, we investigated Eq. (2), through the RH problem and constructed an RH problem under non-zero boundary conditions. By studying the RHP, we derived multiple soliton solutions for the simple poles of Eq. (2). Subsequently, we examined the dynamics of solitons and discussed parameters $\sigma(t)$ and $\gamma_1(t)$ on soliton motion through parameter modulation. We observed that they generally did not influence the amplitude, but they did affect in cases where the soliton velocity was zero or when they took trigonometric function values.

The discussion of soliton motion primarily involved manipulating the values of non-variable coefficients to induce cases of zero and non-zero velocities, and exploring interesting nonlinear phenomena by adjusting the variable coefficients $\sigma(t)$ and $\gamma_1(t)$. Figures 1–7 illustrated soliton motion when $N_2 = 1$, revealing a pair of bright–dark solitons. When $\sigma(t)$ and $\gamma_1(t)$ were modified to different basic functions, corresponding changes in soliton velocity occurred. Figures 8–12 showcased soliton motion when $N_1 = 1$, unveiling various intriguing nonlinear phenomena such as variable-period breathing solitons, parabolic breathing solitons and cubic breathing solitons. Notably, when velocity was zero, altering $\sigma(t)$ and $\gamma_1(t)$ solely affected the soliton's period, resulting in periodic shape variations according to fundamental function rules, with no changes in velocity or peak amplitude. However, when velocity was non-zero, the direction and value of the soliton's velocity varied according to respective functions. Figures 13–16 illustrated soliton interactions under simple poles and $N_3 = 2$, revealing two distinct interaction scenarios: interactions between dark solitons and interactions between bright solitons. Figure 14 presented a set of intriguing nonlinear phenomena, where adjusting parameters caused dark solitons transforming into breathing solitons, while bright solitons mutually canceled each other out, resulting in annihilation. Figures 15 and 16 demonstrated changes induced by modifying $\sigma(t)$ and $\gamma_1(t)$, revealing that changes in velocity before collision adhered to corresponding basic function rules.

The results may deepen the understanding about nonlinear wave phenomena, and provide guidance for specific applications in fiber optic communications. In addition, some other interesting phenomena were observed in Figs. 17–26 when we choose the appropriate values of the coefficients.

Acknowledgements

Project supported by the Natural Science Foundation of Hebei Province, China (Grant No. A2021502004) and the

Fundamental Research Funds for the Central Universities (Grant No. 2024MS126).

References

[1] Wazwaz A M and Kaur L 2019 *Nonlinear Dynam.* **97** 83
[2] Biswas A, Khan K, Rahman A, Yildirim A, Hayat T and Aldossary O M 2012 *J. Optoelectron. Adv. Mater.* **14** 571
[3] Wazwaz A M 2018 *Nonlinear Dynam.* **94** 2655
[4] Gao X Y 2024 *Chin. J. Phys.* **86** 572
[5] Wang H, Yang H, Tian Y and Liu W 2024 *Chaos* **34** 053125
[6] Lakshmanan M, Porsezian K and Daniel M 1988 *Phys. Lett. A* **133** 483
[7] Wang L H, Porsezian K and He J S 2013 *Phys. Rev. E* **87** 069904
[8] Gao X Y 2024 *Appl. Math. Lett.* **152** 109018
[9] Degasperis A and Lombardo S 2013 *Phys. Rev. E* **88** 052914
[10] Agrawal G P 2001 *Nonlinear fiber optics* (San Diego: Academic Press)
[11] Chen J and Feng B F 2023 *Stud. Appl. Math.* **150** 35
[12] Chen J, Yang B and Feng B F 2023 *Stud. Appl. Math.* **151** 1020
[13] Wang H, Zhou Q, Yang H, Meng X, Tian Y and Liu W 2023 *Proc. R. Soc. A* **479** 20230601
[14] Du Z, Tian B, Chai H P, Sun Y and Zhao X H 2018 *Chaos, Solitons and Fractals* **109** 90
[15] Li M Z, Tian B, Qu Q X, Chai H P, Liu L and Du Z 2017 *Superlattice. Microst.* **112** 20
[16] Jia R R and Wang Y F 2022 *Wave Motion* **114** 103042
[17] Guan X, Yang H, Meng X and Liu W 2023 *Appl. Math. Lett.* **136** 108466
[18] Ma L N, Li S, Wang T M, Xie X Y and Du Z 2023 *Phys. Scripta* **98** 075222
[19] Zhu J, Wang L and Geng X 2018 *Front. Math. China* **13** 1245
[20] Zhang Y, Rao J, Cheng Y and He J 2019 *Physica D* **399** 173
[21] Kraus D, Biondini G and Kovačič G 2015 *Nonlinearity* **28** 3101
[22] An L, Ling L and Zhang X 2024 *Physica D* **458** 133888
[23] Kudryashov N A, Kutukov A A and Lavrova S F 2024 *Commun. Nonlinear Sci. Numer. Simul.* **128** 107645
[24] Ling L and Zhang X 2024 *Physica D* **457** 133981
[25] Ju L, Zhang Y, Afzal F and Feng B 2024 *Mod. Phys. Lett. B* **38** 2350254
[26] Rani S, Dhiman S K and Kumar S 2024 *Opt. Quant. Electron.* **56** 532
[27] Luesink E, Ephrati S, Cifani P and Geurts B 2024 *Adv. Contin. Discret. M* **2024** 1
[28] Chen Y X 2023 *Chaos, Solitons and Fractals* **169** 113251
[29] Xu S Y, Zhou Q and Liu W 2023 *Nonlinear Dynam.* **111** 18401
[30] Chen J, Song J, Zhou Z and Yan Z 2023 *Chaos, Solitons and Fractals* **176** 114090
[31] Geng K L, Mou D S and Dai C Q 2023 *Nonlinear Dynam.* **111** 603
[32] Zhang Y and Lin B 2024 *Nonlinear Dynam.* **112** 1
[33] Cotti G 2024 *J. Lond. Math. Soc.* **109** e12860
[34] Geng X, Liu W and Li R 2024 *J. Differ. Equations* **386** 113
[35] Li S, Xia T and Wei H 2023 *Chin. Phys. B* **32** 040203
[36] Novikov S, Manakov S V, Pitaevskii L P and Zakharov V E 1984 *Theory of solitons: the inverse scattering method* (Springer Science and Business Media)
[37] Ablowitz M J, Ablowitz M, Clarkson P and Clarkson P A 1991 *Solitons, Nonlinear Evolution Equations and Inverse Scattering* (Cambridge University Press)
[38] Peng W Q and Chen Y 2022 *Physica D* **435** 133274
[39] Ma W X 2023 *Physica D* **446** 133672